SIAM J. Applied Dynamical Systems
Vol. 3, No. 4, pp. 525–573

On Energy Surfaces and the Resonance Web*

Anna Litvak-Hinenzon† and Vered Rom-Kedar‡

Abstract. A framework for understanding the global structure of near-integrable n DOF Hamiltonian systems is proposed. To this aim two tools are developed—the energy-momentum bifurcation diagrams and the branched surfaces. Their use is demonstrated on a few near-integrable 3 DOF systems. For these systems possible sources of instabilities are identified in the diagrams, and the corresponding energy surfaces are presented in the frequency space and by the branched surfaces. The main results of this formulation are theorems which describe the connection between changes in the topology of the energy surfaces and the existence of resonant lower dimensional tori.

Key words. near-integrable Hamiltonians, parabolic resonances

AMS subject classifications. 70H08, 37J20

DOI. 10.1137/030600106

1. Introduction.

The study of the structure of energy surfaces of integrable systems and the study of resonances and instabilities in near-integrable systems developed into vast disparate research fields. The relation between the two received very little attention. Indeed, near regular level sets of the integrable Hamiltonian, the standard Arnold-resonance web structure appears, and the relation between the two fields reduces to the study of Arnold conjecture regarding instabilities in phase space. Here, we demonstrate that near singular level sets of the integrable Hamiltonian much information regarding possible instabilities of the near-integrable case may be deduced from the structure of the energy surface and its relations with resonance surfaces. We suggest that by adding some information to the traditional energy-momentum diagrams [7], which we name energy-momentum bifurcation diagrams (EMBD), one achieves a global qualitative understanding of the near-integrable dynamics. We relate the geometric properties of the surfaces corresponding to lower dimensional tori in this diagram to both bifurcations in the energy surface topology and the appearance of lower dimensional resonant tori.

Recall that energy surfaces of generic integrable Hamiltonian systems are foliated almost everywhere by n-tori,[1] which may be expressed locally as a product of n circles on which the dynamics reduces to simple rotations (the action-angle coordinates). A given compact regular level set (the set of phase space points with given values of the constants of motion) may be composed of several such tori. The energy surface is composed of all level sets with the same

*Received by the editors March 23, 2003; accepted for publication (in revised form) by T. Kaper May 24, 2004; published electronically November 9, 2004.
http://www.siam.org/journals/siads/3-4/60010.html
†Mathematics Institute, University of Warwick, Coventry CV4 7AL, UK (litvak@maths.warwick.ac.uk). This author was partially supported by the Marie Curie Individual Fellowship HPMF-CT-2002-01742 and an INTAS grant.
‡Faculty of Mathematical and Computer Science, Weizmann Institute, Rehovot 76100, Israel (vered@wisdom.weizmann.ac.il). This author acknowledges the support of The MINERVA Foundation.
[1]For simplicity we consider here only the case of compact level sets.

energy. If these iso-energy level sets have different numbers of components, then there exists a singular level set on this energy surface which is not smoothly conjugate to a collection of n-tori. Under quite general conditions, Lerman and Umanskii [33] show that by using the reduction procedure [1] and Nehorošev results [42], such a connected singular level set may be expressed locally as an $n-s$ dimensional torus with frequencies depending on $n-s$ actions crossed with a fixed point and its asymptotic manifolds in the remaining s DOF subsystem ($s \leq n$). This s DOF subsystem is called the normal system and its structure generally depends on the $n-s$ actions. (See exact statements in the formulation section below. For a complete treatment see [33].) The regular n-tori correspond to the case $s=0$. The larger the s the more cases and possibilities one has for the behavior in the normal directions. The larger the $n-s$, the more possibilities to transfer between the different cases, namely, to encounter bifurcations. In this context, the Lerman and Umanskii work [33] is mainly concerned with $n=s=2$, and the Lerman work [29] is mainly concerned with $n=s=3$ (yet it includes the generic bifurcation diagrams for the $s=1,2$ cases), whereas the works of Oshemkov [43], Fomenko [16], and Bolsinov and Fomenko [4] are mainly concerned with $n=2$, $s=1$. Here, we consider $s=1$ and $n \geq 2$, studying the implications of phase space bifurcations and resonances as a source for instabilities in the near-integrable systems.

Our main result, Theorem 2 (section 8.2), roughly states that *the existence of a nondegenerate $n-1$ dimensional torus of fixed points implies bifurcations in the topology of the energy surface*. Furthermore we prove that such a torus appears as an extrema of certain surfaces in the EMBD. In other words, this provides a relation among energy surface topology, bifurcations in the EMBD, and lower dimensional resonant tori.

The local coordinate representation of the lower dimensional singular tori naturally leads to investigation of critical points of the Hamiltonian function in the normal plane, with the remaining $n-s$ actions viewed as parameters [42]. Hence, as shown in [33, 29] and more recently in [25], for small $n-s$, singularity theory may be used to classify all generic bifurcations (or all generic bifurcations under given symmetries [25]) in the s DOF subsystem. Here we consider, in addition to the above bifurcations, extrema in the action variables of the Hamiltonian function evaluated along the singularity surfaces. We relate these extrema to strong resonances. A complete classification of all generic scenarios (of combinations of resonances and bifurcations in the normal plane), using singularity theory, is yet to be developed.

Since the integrable system has n integrals of motion, a representation of the energy surfaces corresponds to indicating the range of allowed motion and its character in some n dimensional space (the innocent words "its character" hide a vast body of work dedicated to understanding the topology of the level sets which are represented as points in this reduced space as discussed below). Traditional spaces for such representation are the frequency domain [27], the space of constants of motion (e.g., [2, 33, 40, 18, 17]), the energy-momentum space, and the momentum space (e.g., [2, 1, 6, 7, 47, 10, 33, 40]). Such presentations are all equivalent near regular level sets, where action-angle coordinates may be introduced. Furthermore, each of these representations is inherently nonunique as one may choose any nonsingular vector function of the conserved quantities to serve as the new set of coordinates. We propose that a convenient representation appears in a specific combination of energy and momentum space. Convenient here means the following.

C1. The geometric presentation supplies a concise summary of all the dynamics and geomet-

rical features of the integrable system for all energy levels.

C2. The geometric presentation provides clear criteria for the location of special regions in phase space which are expected to produce strong instabilities under a given form of a perturbation.

While many presentations in the n dimensional space satisfy the first criteria, it appears that the second one has not been explicitly addressed. Notice that the first criteria deals with the integrable part of the Hamiltonian only. On the other hand, the second one depends on the nature of the applied perturbation; hence *the choice of the most convenient representation of the integrable system depends on the form of the perturbation.* These issues are explained more fully in section 4, where we propose a choice of convenient coordinates. A similar approach, in which the perturbation determines the appropriate integrable system, is taken in the partial averaging procedure. Other related works, in which the geometry of the energy surfaces and their intersection with the resonance web are related to the perturbed dynamics, are those on "resonance streaming," where it is argued that in 2 DOF integrable systems a small angle between the intersecting resonance and energy curves (plotted in the frequency space) enhances the effect of added noise [34, 48].

The various representations in the n dimensional spaces of the constants of motion identify the regions of the allowed motion but do not, in general, supply information regarding the topology of the level sets. Indeed, the classification of all the possible topologies of the level sets of energy surfaces of integrable Hamiltonians is extremely challenging (see [2, 33, 40, 17, 1, 47]) and has been completed for the 2 DOF case only [17, 33]. Lerman and Umanskii use the $n = 2$ integrals of motion near fixed points to obtain local and global information regarding the level sets of the integrable motion and to classify all possible generic homoclinic connections which are induced by the local behavior [30, 31, 32]. We use their formulation in our treatment of lower dimensional tori. Fomenko and coworkers suggested using graphs to represent all topologically distinct tori which appear in the integrable dynamics [17, 18, 16, 43, 4]. Some of these ideas have been extended to classify integrable 3 DOF dynamics such as the motion of rigid body [17, 10, 11]. Oshemkov, Fomenko, and coworkers use the 2 DOF constructions on given level sets of the third integral to analyze such systems [43, 17, 18], though Fomenko had also formulated a higher dimensional generalization of his theory [17]. Dullin et al. (see, e.g., [10, 11, 51] and references therein) have shown that such approaches may be used to develop schemes for computing action-angle coordinates even when the topology of the energy surfaces is complicated and finding n topologically independent circles (n circles which are irreducible to each other) is an a priori complicated task. Here we investigate the structure of energy surfaces with *very simple* topological structure for which we are able to generalize Fomenko–Oshemkov graphs to branched surfaces. These branched surfaces may be viewed as simple examples of Fomenko's higher dimensional theory.

The paper is ordered as follows: in section 2 we describe the type of the near-integrable Hamiltonians we study, with prototype examples of 3 DOF systems which demonstrate the appearance of nontrivial energy surfaces. In section 3 we formulate the notions of branched surfaces, topological bifurcations of the energy surfaces, and the EMBD. In section 4 we propose a convenient choice of momentum and explain how the choice of suitable coordinates depends on the form of the perturbation. In section 5 we describe the structure of the energy surfaces and the resonance web in the frequency space and in the energy momentum space

near normally elliptic lower dimensional tori. The integrable structure in this a priori stable case is trivial and we add essentially no new insights to the known results. It is included here to build intuition for the next two sections. In section 6, we describe these structures near level sets corresponding to normally hyperbolic invariant $(n-1)$-tori. In section 7 we proceed to describe these structures near normally parabolic tori. In section 8 we prove our main theorems relating resonances and bifurcations. We conclude with a discussion section.

2. Formulation. Consider a near-integrable Hamiltonian $H(q,p;\varepsilon) = H_0(q,p)+\varepsilon H_1(q,p;\varepsilon)$, $\varepsilon \ll 1$, $(q,p) \in M \subseteq \mathbb{R}^n \times \mathbb{R}^n$, where M is a $2n$ dimensional smooth symplectic manifold and H_0, H_1 are C^∞ (smooth).[2] We further assume that there exists $\varepsilon_0 > 0$ such that H_1 is bounded[3] for all real values of $(q,p;\varepsilon)$ for $\varepsilon \in [0,\varepsilon_0]$. H_0 represents the completely integrable part of the Hamiltonian (the unperturbed system) and its structure is described below. For any ε, a perturbed orbit with energy h resides on the energy surface $H_0(\cdot) = h - \varepsilon H_1(\cdot;\varepsilon)$. Hence, by assumption, the structure of the unperturbed energy surfaces and their resonance webs in an $O(\varepsilon)$-interval of energies near h supplies global information on the allowed range of motion of the perturbed orbits.

The integrable n DOF Hamiltonian, $H_0(q,p)$; $(q,p) \in M \subseteq \mathbb{R}^n \times \mathbb{R}^n$, has n integrals of motion, $H_0 = F_1, F_2, \ldots, F_n \in C^\infty(M)$, which are functionally independent at almost all points of M and are pairwise in involution: $\{F_i, F_j\} = 0$; $i,j = 1,\ldots n$. Assume that $n \geq 3$ and that the Hamiltonian level sets, $M_g = \{(q,p) \in M, \quad F_i = g_i; \quad i = 1,\ldots,n\}$, are compact (this assumption implies, in particular, that the set $F_1, F_2, \ldots, F_n$ is complete; see [33]). By the Liouville–Arnold theorem (see [42] and [2, 26]), the connected compact components of the level sets M_g, on which all of the dF_i are (pointwise) linearly independent, are diffeomorphic to n-tori, and hence a transformation to action-angle coordinates ($H_0 = H_0(I)$) near such level sets is nonsingular. Consider a neighborhood of a level set M_{g0} which possibly contains a singularity set at which s of the dF_i's are linearly dependent; on each connected and closed component of such a Hamiltonian level set there is some neighborhood D, in which the Hamiltonian $H_0(q,p)$ may be transformed by the reduction procedure to the form (see [33], [42])

$$H_0(x,y,I), \qquad (x,y,\theta,I) \in U \subseteq \mathbb{R}^s \times \mathbb{R}^s \times \mathbb{T}^{n-s} \times \mathbb{R}^{n-s}, \tag{2.1}$$

which does not depend on the angles of the tori, θ. The symplectic structure of the new integrable Hamiltonian (2.1) is $\sum_{j=1}^{s} dx_j \wedge dy_j + \sum_{i=1}^{n-s} d\theta_i \wedge dI_i$, where (x,θ,I) are the generalized action-angle variables ($s=0$ corresponds to the maximal dimensional tori—the n-tori discussed above). The motion on the $(n-s)$ dimensional family (parameterized by the actions I) of $(n-s)$-tori is described by the equations

$$\dot{\theta}_i = \omega_i(x,y,I), \quad \dot{I}_i = 0.$$

The geometrical structure of the new Hamiltonian, $H_0(x,y,I)$, is such that for any fixed I ($I = (I_1,\ldots,I_{n-s})$) an $(n-s)$-torus is attached to every point of the (x,y) plane (space, for

[2] One may relax these requirements to the C^r case, but this is left for future studies.

[3] It is probably sufficient to assume that for large (q,p) H_1 does not grow faster than H_0, namely, that for $\varepsilon_0 > 0$ sufficiently small there exist constants $C_1, C_2 \geq 0$ such that $|H_1(q,p;\varepsilon)| < C_1 + C_2\,|H_0(q,p)|$ for all $(q,p) \in M$ and $\varepsilon \in [0,\varepsilon_0]$, but we leave the details of this case for future work.

$s > 1$). The (x, y) plane (space) is called the *normal plane* (*space*) [2, 44, 3] of the $(n-s)$-tori and defines their stability type in the normal direction to the *family*[4] of tori. Invariant lower dimensional tori, of dimension $(n-l)$, generically exist for each $1 \le l \le n-1$; indeed, for any given s consider an m-resonant value of I. Then, for each such I, there exists an m dimensional family (corresponding to different initial angles) of $n-s-m$ dimensional tori. All these tori belong to the higher $n-s$ dimensional resonant torus, associated with I. The existence of such lower dimensional tori is restricted to the $n-s-m$ dimensional resonant surface of I values. A different type of lower dimensional invariant tori, which are of the main interest here, corresponds to isolated fixed point(s) of the s dimensional normal space. These appear on an $n-s$ dimensional manifold of I values, the singularity manifold (such a generalized fixed point corresponds to a manifold on which each dF_i for $i = 1, \ldots, s$ is linearly dependent on $dI_1, \ldots, dI_{n-s}$, where $dI_1, \ldots, dI_{n-s}$ are pointwise linearly independent). Locally, one may choose the (x, y, I) coordinate system so that for these tori

$$\nabla_{(x,y)} H_0(x, y, I)\big|_{p_f} = 0, \qquad p_f = (x_f, y_f, I_f). \tag{2.2}$$

Following the terminology of [33], the invariant tori on which (2.2) is satisfied are called here singular tori, and the manifolds of action values on which this equation is satisfied are called singularity manifolds. The structure of these is discussed in the next section.

Hereafter, consider the case $s = 1$ only. The invariant $(n-1)$-tori have an $(n-1)$ dimensional vector of inner frequencies, $\dot{\theta} = \omega(p_f)$. The normal stability type of such families of $(n-1)$-tori is determined by the characteristic eigenvalues (resp., Flouqet multipliers for the corresponding Poincaré map) of the linearization of the system about the tori; generically, these tori are either normally elliptic[5] or normally hyperbolic.[6] If the torus has one pair of zero characteristic eigenvalues in the direction of the normal (x, y) space, it is said to be *normally parabolic*. In addition, the *normal frequency*[7] [2, 44], Ω, of the $(n-1)$-tori is defined as the (nonnegative) imaginary part of the purely imaginary characteristic eigenvalues.[8]

Locally, in the (x, y, I) coordinate system, the normal stability of the invariant torus is determined by

$$\det\left(\frac{\partial^2 H_0}{\partial^2(x, y)}\bigg|_{p_f}\right) = -\lambda_{p_f}^2, \tag{2.3}$$

where p_f satisfies (2.2). Indeed, when λ_{p_f} is real and nonvanishing the corresponding family of tori is said to be normally hyperbolic, when it vanishes it is called normally parabolic, and when it is pure imaginary it is normally elliptic. For more details on the above see [33, 2, 5, 12, 13, 14, 15, 21, 22, 23, 24, 26, 44, 3] and references therein.

[4]Notice that a single torus belonging to this family has neutral stability in the actions directions. The normal stability referred to in the Hamiltonian context ignores these directions; see [5, 3] and references therein.

[5]If all the characteristic eigenvalues of an invariant lower dimensional torus (with respect to its normal (x, y) space) are purely imaginary (and do not vanish), it is said to be *normally elliptic*.

[6]If all the characteristic eigenvalues of an invariant lower dimensional torus (with respect to its normal (x, y) space) have a nonzero real part, it is said to be *normally hyperbolic*.

[7]In some references, these are called characteristic frequencies.

[8]In some references, e.g., [5], the normal frequencies are defined as the positive imaginary parts of the characteristic eigenvalues.

An example of a 3 DOF integrable Hamiltonian which is in the form (2.1), possesses families of invariant 2-tori of all three normal stability types (elliptic, hyperbolic, and parabolic) at $x = y = 0$, and satisfies all the stated above assumptions is

$$H_{bif}(x, y, I_1, I_2) = \frac{y^2}{2} - \frac{x^2}{2} I_1 + \frac{x^4}{4} + \left(\mu_1 + \frac{1}{2}\right) \frac{I_1^2}{2} + \frac{I_2^2}{2} + \alpha_2 I_2 + \alpha_3 I_1 I_2, \tag{2.4}$$

where α_2, α_3, and μ_1 are fixed parameters. Notice that this Hamiltonian has a Z_2 symmetry in the (x, y) coordinates. We will comment in the text when these symmetries play a role. In fact, the form of 3 DOF integrable Hamiltonian families in general position having a parabolic 2-tori has been derived (see [16],[33]). A complete study of their structure will be discussed elsewhere. We may compare it to a standard model of (Z_2 symmetric) a priori stable systems with bounded energy surfaces having a family of normally elliptic 2-tori at $x = y = 0$,

$$\begin{aligned} H_{st}(x, y, I_1, I_2) &= \frac{y^2}{2} + \frac{x^2}{2} + \frac{1}{8}\left(x^2 + y^2\right)^2 + \alpha_1 I_1 + \alpha_2 I_2 + \frac{I_1^2}{2} + \frac{I_2^2}{2} \\ &= \sum_{i=0}^{2} \left(\alpha_i I_i + \frac{I_i^2}{2}\right), \qquad \alpha_0 = 1, \end{aligned} \tag{2.5}$$

and to the corresponding (symmetric) a priori unstable system

$$H_{ust}(x, y, I_1, I_2) = \frac{y^2}{2} - \frac{x^2}{2} + \frac{x^4}{4} + \alpha_1 I_1 + \alpha_2 I_2 + \frac{I_1^2}{2} + \frac{I_2^2}{2}, \tag{2.6}$$

which has a family of normally hyperbolic 2-tori at $x = y = 0$.

In sections 5, 6, 7, the representative models (2.5), (2.6), and (2.4) are studied in detail. In particular, for each of these models we construct the EMBD, find the branched surfaces which supply a representation for the energy surfaces geometry, and plot representing energy surfaces in the frequency plane. Below we define the branched surfaces and the EMBD. Some readers may find it helpful to read sections 5, 6, 7 first.

3. EMBD and branched surfaces. Fomenko and his coworkers have developed a sophisticated representation of integrable 2 DOF systems which leads to their orbital classification. Roughly, on each energy surface, they have suggested representing families of regular 2-tori by edges of a graph, whereas singular surfaces at which such families coalesce or undergo a change of orientation correspond to the vertices of the graph. The vertices corresponding to singular level sets are labeled according to the orbital changes they represent: "type A molecules" are vertices corresponding to normally elliptic circles, and "type B molecules" are vertices corresponding to a normally hyperbolic circle and its figure eight separatrices. Starred molecules correspond to change of orientation. To deal with higher dimensional systems, Fomenko and Oshemkov have suggested constructing tables of the 2 DOF molecules which list how these graphs vary as the constants of motion are changed. Other setups, closer to our construction, were suggested by Fomenko in [17] but, to the best of our knowledge, have not been examined or used for any specific model. Here, we explicitly construct the branched surfaces which we view as a different type of generalization of the simplest form (molecules A and B) of the Fomenko graphs.

Consider an integrable n DOF Hamiltonian on a $2n$ dimensional symplectic manifold M and its associated n integrals of motion $H_0 = F_1, F_2, \ldots, F_n$. We call the set of constants of motion *valid* if they are *almost everywhere* functionally independent on M, are pairwise in involution, and are complete. Denote by A_h the set of allowed values of $F_2, \ldots, F_n$ on the energy surface $E_h = \{(q,p)|\ H_0(q,p) = h\}$, namely, $A_h = \{(g_2, \ldots g_n)|\ M_{(h,g_2,\ldots g_n)} \neq \emptyset\}$ (recall that the level set M_g is defined as $M_g = \{(q,p) \in M, \quad F_i = g_i; \quad i = 1, \ldots, n\}$). It follows that $E_h = \cup_{(g_2,\ldots g_n)\in A_h} M_{(h,g_2,\ldots g_n)}$. Let $k(g)$ denote the number of disconnected components of M_g, so $M_{(h,g_2,\ldots g_n)} = \biguplus_{j=1}^{k(h,g_2,\ldots g_n)} l_j^{(h,g_2,\ldots g_n)}$, where l_j^g denotes a connected component of M_g. Fixing h, $k(h, g_2, \ldots g_n)$ is constant when the level sets $M_{(h,g_2,\ldots g_n)}$ deform smoothly with $g_2, \ldots g_n$ (namely, at $h, g_2, \ldots g_n$ the energy-momentum mapping is a trivial fiber bundle; see [2, 47]). Recall (see section 2) that the singularity surfaces of A_h are defined as the values of $(g_2, \ldots g_n)$ for which there exists a point $(q,p) \in M_{(h,g_2,\ldots g_n)}$ at which s of the dF_i are linearly dependent and the rank of the n vectors dF_i at the singularity is $n - s$. Let us denote the union of the singularity surfaces of some given A_h by A_h^S. For any finite range of (h, g) values, by the assumption on the compactness of the level sets, $k(h, g_2, \ldots g_n)$ may change only across a singular level set, and hence

$$A_h^S \supseteq A_h^{GS} = \{(g_2, \ldots g_n)|\ k(h, g_2, \ldots g_n) \text{ is discontinuous in } g_2, \ldots g_n\}.$$

Equality of these sets is expected in the generic case with $s = 1$. Nongeneric (e.g., symmetric) coincidences, by which disconnected level sets coincide and split at the same g value, may be similarly treated and will be ignored here (see [18] and [33] for discussion). The behavior of $k(h, g_2, \ldots g_n)$ near singular level sets with $s \geq 2$ will be studied elsewhere.

We remark that Smale [47, 2] has called the values at which the energy-momentum map is not locally trivial in the differentiable sense (such as A_h^S) the bifurcation set—these values correspond to changes in the topology of the *level sets*. We follow here the Lerman and Umanskii terminology, referring to A_h^S as the singularity set, and we reserve the term bifurcation for changes in the energy surfaces structure (see Definition 3), which is the main focus of the current work.

Define a function $S_h : E_h \to \mathbb{R}^n$ as (recall that $g_1 = h$)

$$S_h(q,p) = (\delta(q,p), g_2, \ldots g_n), \text{ where } F_i(q,p) = g_i,\ i = 1, \ldots, n,$$

where the scalar function $\delta(q,p)$ satisfies the following:

- $\delta(q,p) = 0$ iff $k(g(q,p)) = 1$;
- two points belonging to the same level set have the same δ iff they belong to a connected component of M_g,

$$\{(q,p),(q',p') \in M_g \text{ and } \delta(q,p) = \delta(q',p')\} \Leftrightarrow (q,p),(q',p') \in l_j^g;$$

- $\delta(q,p)$ is smooth (C^r for some $r \geq 1$) for all $(q,p) \in E_h$ with $(g_2, \ldots g_n) \in A_h \backslash A_h^S$, and $\delta(q,p)$ is continuous for $(g_2, \ldots g_n) \in A_h$.

Hence, on each level set M_g, $\delta(q,p)$ (with $g = F(q,p)$) attains exactly $k(g)$ distinct values, i.e.,

$$\{\delta(q,p)|\ (q,p) \in M_g\} = \{\delta_1(g), \ldots, \delta_{k(g)}(g)\}$$

and $\delta_i(g) \neq \delta_j(g)$ for $i \neq j$. Therefore, we may define

$$\delta(l_j^g) = \delta(q,p)|_{(q,p)\in l_j^g} = \delta_j(g),\ j = 1,\dots,k(g),$$

and hence

$$S_h(l_j^g) = S_h(q,p)|_{(q,p)\in l_j^g} = (\delta_j(g), g_2, \dots g_n).$$

Furthermore, if l_j^g and l_i^g coalesce to a (singular) level set $l_k^{g^*}$ as $g \to g^*$, then $\delta(l_{i,j}^g) \to \delta(l_k^{g^*})$. Summarizing, there is a 1-1 correspondence between the range of S_h and the connected components of the level sets in E_h, and this correspondence depends continuously on the phase space points even across singularities. In particular, if the level sets are compact, every point at which $S_h(q,p)$ is smooth corresponds to a single n-torus, and every point at which $S_h(q,p)$ is not smooth corresponds to a singular level set. Applying the above procedure for $n = 2$ leads immediately to the construction of the Fomenko graphs.

Definition 1. *The branched surface of an energy surface E_h is given by the surface $S_h(E_h)$; namely, it is the $n-1$ dimensional surface embedded in $\mathbb{R}^n$: $\mathcal{F} = \{y|\ y = S_h(q,p), (q,p) \in E_h\}$.*

Definition 2. *Two branched surfaces are equivalent if there exists a diffeomorphism of $\mathbb{R}^n$ which maps one branched surface to the other.*

Notice that, by definition, two equivalent branched surfaces are topologically conjugate. We require differentiable conjugacy so that the singular surfaces of two equivalent branched surfaces will be topologically conjugate to each other as well.

Figure 9 demonstrates that such a construction is possible for simple systems with singularities of order 1 (namely, with $s = 1$). These branched surfaces generalize the simplest molecules (A, B) of the Fomenko graphs. The application of this procedure to physical models is under current investigation; it may lead to further development of the theory, generalizing the other types of molecules which were constructed by Fomenko and his coworkers. Whether this will finally lead to a complete classification of integrable higher dimensional systems, as in the 2 DOF case, is unknown to us. First steps in this direction, in a more abstract setting, are included in [17]. In any case, it is easy to see the following.

Corollary 1. *Given an integrable Hamiltonian system, the branched surfaces constructed from two different valid sets of constants of motion (with $H_0 = F_1$) are equivalent.*

In particular, the construction of these surfaces from the EMBD, the frequency space diagram and the constant of motion diagrams are all equivalent, as demonstrated in sections 5, 6, 7.

Nearby energy surfaces correspond usually to a smooth deformations of each other; hence they will usually have equivalent branched surfaces. When nearby energy surfaces have different structures we say that the energy surface has undergone a bifurcation.

Definition 3. *h_c is an energy bifurcation point if the branched surfaces at h_c and at $h_c \pm \varepsilon$ are not equivalent for arbitrarily small ε.*

The EMBD supplies global information on the bifurcations of the energy surfaces structure and their relation to resonances; consider an integrable Hamiltonian system $H_0(q,p)$ in a region $D \subseteq M$ at which a transformation to the local coordinate system $H_0(x,y,I)$ with $s = 1$ is nonsingular. The energy-momentum map assigns to each point of the phase space (x,y,I) a

point in the energy-momentum space $(h = H_0(x, y, I), I)$. The EMBD is a plot in the (h, I) space (for (h, I) in the range of D) which includes

- the region(s) of allowed motion (the closure of all regions in which the energy-momentum mapping is a trivial fiber bundle; see [2, 47]);
- the $s = 1$ singular surfaces $(h, I) = (H_0(p_f), I_f)$ (see (2.2)) where the normal stability of the corresponding singular $(n-1)$-tori, defined by (2.3), is indicated;
- the strongest resonance surfaces on which the inner frequencies of the tori vanish, $\omega_i = 0$, and the regions in which back-flow occurs (where $\dot{\theta}_i(x, y, I)$ changes sign along the level set $(h = H_0(x, y, I), I)$ for some $i = 1, \ldots, n - s$);
- the energies at which topological bifurcations occur and the branched surfaces in the intervals separate by these bifurcation points.

4. The dependence of the EMBD on the form of the perturbation. The EMBD depends on the choice of the generalized action-angle co-ordinates (x, y, I). In particular, a symplectic transformation of the (θ, I) coordinates to other generalized action-angle coordinates (φ, J) may change some geometric properties of this diagram. Furthermore, transformations of the form $(\theta, I) \to (\varphi = \theta - \varpi(I)t, I)$, which correspond to moving relative to particular tori with frequency vectors $\omega = \varpi(I)$, for which $H_{new}(J) = H_0(J) - \overline{H}(J)$ (where $\varpi(I) = \frac{\partial \overline{H}(I)}{\partial I}$), may change the topology of the energy surfaces, the structure of their singularity manifolds, and the nature of their intersections with the resonance hypersurfaces. Hence, it appears that finding the "correct" representation is ill defined in the context of the integrable system. *We propose that the form of the perturbation resolves these issues.*

The role of the form of the perturbation is apparent when one considers the procedure of partial averaging in near-integrable Hamiltonian systems (see [2, p. 173]). First, this procedure implies that if for a given perturbation the number of independent resonant vectors, r, is smaller than the number of angle variables (here $n-1$), then, by averaging over the $n-r-1$ nonresonant directions one can obtain a system which is exponentially close to the $r+1$ dimensional system depending on the $n-r-1$ parameters (the averaged actions). Hence, with no loss of generality, we assume here that the perturbation includes $n-1$ independent resonant directions. Then, it follows that for autonomous systems the transformation $(\theta, I) \to (\varphi = \theta - \varpi(I)t, I)$ produces time-dependent Hamiltonians, and hence $\varpi(I)$ must vanish identically.[9] This trivial statement implies, in particular, that given an a priori stable near-integrable system of the form (2.5), for generic vector α, it may not be transformed to a system with $\alpha = 0$ without introducing time-dependent perturbations.

The second issue which arises is the choice of the action variables, which implicitly determines which resonances are considered strong. This issue is again well understood in the context of partial averaging [2]; the form of the anticipated *perturbation* determines which of the resonant surfaces will produce the strongest response; consider the near-integrable system expressed near a singular level set in some local generalized action-angle coordinates:

$$H(q, p) = H_0(x, y, I) + \varepsilon H_1(x, y, \theta, I). \tag{4.1}$$

[9]Here we need the assumption on having $n-1$ independent resonant relations. Indeed, if $n \geq 3$ and $H_1(x, y, I, \theta) = \cos(\theta_1 - \theta_2)$, one can immediately see that this statement is false.

Consider the Fourier series of H_1:

$$H_1(q,p) = H_1(x,y,\theta,I) = \sum_{|k|=|k_1|+\cdots+|k_n|\geq r_0} h_k(x,y,I)\exp(\mathrm{i}\langle k,\theta\rangle).$$

Then, provided h_k are monotonically decreasing (if H_1 is assumed to be analytic, h_k decays exponentially for large $|k|$, and if H_1 is assumed to be C^r, the decay rate is of order $|k|^{-r}$), the strongest resonances are given by the frequencies satisfying $\langle k,\omega\rangle = 0$ for k values which are included in the sum ($h_k \neq 0$ near the singular level set) and satisfy $|k| \approx r_0$; see [2] for an exact definition and discussion. In particular, by a change of the action angle coordinates $(\theta, I) \to (\varphi, J)$ one may arrange the terms so that the first n terms in the above sum have $k^j = r_j e_n^j = (0,\ldots,r_j,\ldots 0)$ for $j = 1,\ldots,n$ (where r_j is in the jth place, and are monotonically increasing with j). Then, the strongest resonances occur along the action variables directions.

Summarizing the above observations, we propose the following.

Definition 4. *The local generalized action-angle coordinates (x,y,θ,I) of the integrable part of a near-integrable system are called suitable if the following hold:*

- *The perturbed system is autonomous.*
- *The strongest $n-s$ resonant terms are nonzero and are aligned, in decreasing order, along the $n-s$ actions. More precisely, let*

$$H_1(q,p) = H_1(x,y,\theta,I) = \sum_j h_{k^j}(x,y,I)\exp(\mathrm{i}\langle k^j,\theta\rangle), \quad j\in\mathbb{N}, \tag{4.2}$$

with $|k^j|$ monotonically increasing with j and $\|h_{k^j}\|$ monotonically decreasing with j for equal $|k^j|$ values. Then, $k^j \| e_{n-s}^j$ (i.e., k^j is parallel to e_{n-s}^j) for $j = 1,\ldots,n-s$, where e_{n-s}^j is the $n-s$ dimensional unit vector with 1 at the jth entry.

Notice that the sum in (4.2) is assumed to have *at least* $n-s$ terms with $n-s$ independent k^j vectors. In general the sum has an *infinite number* of nonzero terms, where the k^j vectors with $j > n-s$ are linearly dependent on $(k^1,\ldots,k^{n-s})$.

Lemma 1. *If (x,y,θ,I) and (q,p,φ,J) are two suitable coordinate systems for the Hamiltonian (4.1), then $I = J$ and $\varphi = \theta + f(I)$.*

Proof. First, we recall that by generalized action-angle coordinates we assume that near the singular level set the unperturbed equations of motion for (I,θ) are of the form

$$\frac{dI}{dt} = 0 = -\frac{\partial H_0}{\partial\theta}, \quad \frac{d\theta}{dt} = \omega(x,y,I) = \frac{\partial H_0}{\partial I},$$

and similarly for the (J,φ) coordinates. Let $W(J,\theta)$ denote the generating function which transforms (x_f,y_f,θ,I_f) to (q_f,p_f,φ,J_f). Since both θ and φ are angle coordinates, it follows that $W(J,\theta)$ is of the form $W(J,\theta) = J^T R\theta + F(J)$, where R is a unimodular integral matrix (see [2, p. 173]), so that

$$I_f^T = \frac{\partial W}{\partial\theta} = J_f^T R,$$
$$\varphi = \frac{\partial W}{\partial J_f} = R\theta + F'(J_f).$$

In particular, the requirement that both θ and φ are 2π periodic in all their arguments and that the transformation is smooth implies that R is a constant integral matrix, independent of J_f. Furthermore, extending the transformation to a neighborhood of the singular level set must still preserve this property. To complete the proof, we need to show that $R = Id$. Indeed, expressing the perturbed part of the Hamiltonian in the (x, y, θ, I) coordinates and using the above transformation in (4.2), we obtain

$$H_1(q, p, \varphi, J) = \sum_j \widetilde{h_{k^j}}(q, p, J) \exp(\mathrm{i} \left\langle k^j, R^{-1}\varphi \right\rangle), \quad j \in \mathbb{N},$$

with $k^j || e^j_{n-s}$ for $j = 1, \ldots, n-s$ (where R^{-1} is a unimodular integral matrix as well). Therefore, insisting that q, p, φ, J are suitable implies that for all φ

$$\left\langle e^j_{n-s}, R^{-1}\varphi \right\rangle = \left\langle e^j_{n-s}, \varphi \right\rangle \quad \text{for} \quad j = 1, \ldots, n-s$$

and hence that $R^{-1} = R = Id$. ■

Conversely, one may take the usual convention by which, given an integrable Hamiltonian in a given coordinate system, the analysis determines which form of the perturbation will cause the largest instability in the vicinity of a given resonance junction. In particular, by the appropriate change of coordinates of the integrable system, one obtains that the *strongest* resonances possible are realized when $k = e^j_n = (0, 0, \ldots, 0, 1, 0, \ldots, 0)$. With this view the notion of strongest resonances is inherently coordinate-dependent.

In our presentation of the energy surfaces in the energy-momentum plots we relate changes in the energy surface singular structures to strong resonances of lower dimensional tori and to instabilities in the near-integrable system. To make such statements well defined, we insist that the coordinates we use are locally suitable coordinates. On the other hand, results which relate strong resonances to topological changes in the energy surfaces (e.g., Theorem 2) are independent of the choice of the coordinate system.

5. A priori stable systems.

To obtain a good understanding of the proposed presentation of the EMBD we begin with the simplest and most familiar model of a priori stable systems near the lower dimensional torus. Let us examine the presentation of the regular part of the energy surface first in the frequency space and then in the energy-momentum space.

5.1. Energy surfaces in the frequency space (S).

For the standard Hamiltonian H_{st} (see (2.5)) the transformation from momentum to frequency variables is a shift ($\omega(I) = \alpha + I, \quad \alpha = (1, \alpha_1, \alpha_2)$) and is regular everywhere, so we can write

$$H_{st}(I) = H_{st}(\omega) = \frac{1}{2} \|\omega(I)\|^2 - \frac{1}{2} \|\alpha\|^2, \tag{5.1}$$

and we obtain the standard result that in the definite case the energy surfaces appear in the frequency space as spheres centered at $\omega = 0$. The natural oscillations near the elliptic fixed point $x = y = 0$ (where the transformation from the (x, y) coordinates to the action-angle coordinates is singular) correspond to the circle $\omega_0 = \alpha_0 = 1$, and in this representation appear as a regular level set of the energy surface. Here it is natural to insist on positive I_0 value,

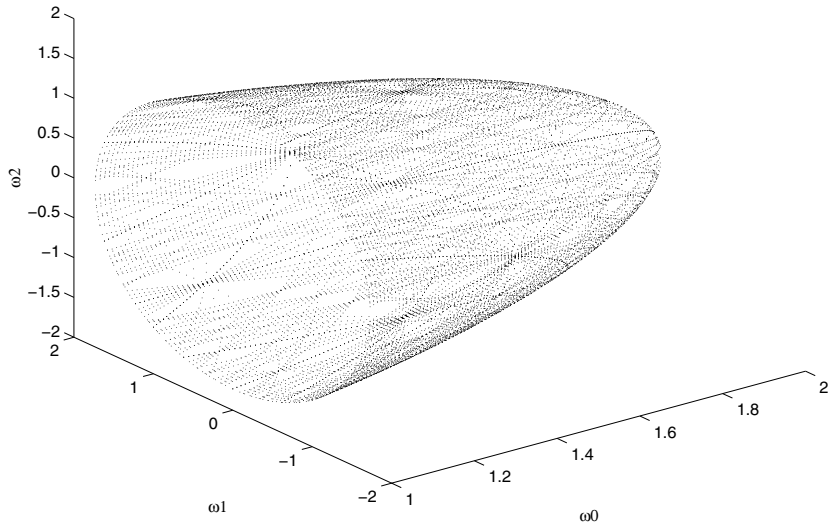

Figure 1. *A resonance web on a cap of an energy surface of an a priori stable system (* (5.1) *with* $h = 0.5$*).*

leading to energy surfaces in the form of "caps" with boundaries: $\omega^h = \{\omega |\ \|\omega\|^2 = 2h + \|\alpha\|^2, \omega_0 \geq \alpha_0 = 1\}$. The boundary $\omega_0 = \alpha_0$ corresponds to the family of lower dimensional tori $x = y = 0$ on the given energy surface; see Figure 1. In the figure we also show the dense intersection of the resonance surfaces, given by planes passing through the origin, with this cap (see [2, 23, 34] and references therein). The planes $\omega_i \equiv 0,\ i = 0, 1, 2$, correspond to the strongest resonances. Notice that the only energy surface which includes the origin is a sphere with diminishing radius, and such an energy surface is disallowed for systems of the form (5.1) since[10] $\|\alpha\| \neq 0$.

5.2. Energy surfaces in the energy-momentum space (S). In Figure 2, we construct the EMBD of the system (2.5) by presenting the energy surfaces in the space (H_0, I_1, I_2), where $H_{st}(x, y, I) = H_0$. For any given energy $H_0 = h$, the allowed region of motion is bounded by the family of normally elliptic 2-tori $(x, y, I) = (0, 0, I(h))$. The corresponding singularity surface in the EMBD is given by the paraboloid

$$p^0_{ell}(h, I_1, I_2) = \left\{ (h, I_1, I_2) |\quad H_{st}(0, 0, I) = \frac{1}{2}\sum_{i=1}^{2} \left((\alpha_i + I_i)^2 - \alpha_i^2 \right) = h,\ h \geq h_{ell} = 0 \right\};$$

namely, for a given h, (I_1, I_2) belong to a circle of radius $\sqrt{2h + \alpha_1^2 + \alpha_2^2}$ which is centered at $(-\alpha_1, -\alpha_2)$.The singularity manifolds corresponding to *normally elliptic* invariant tori are denoted by a collection of *solid* curves in the EMBD as demonstrated in Figure 2. To see that

[10]Recall that changing α corresponds to considering perturbations which are quasi-periodic functions of time.

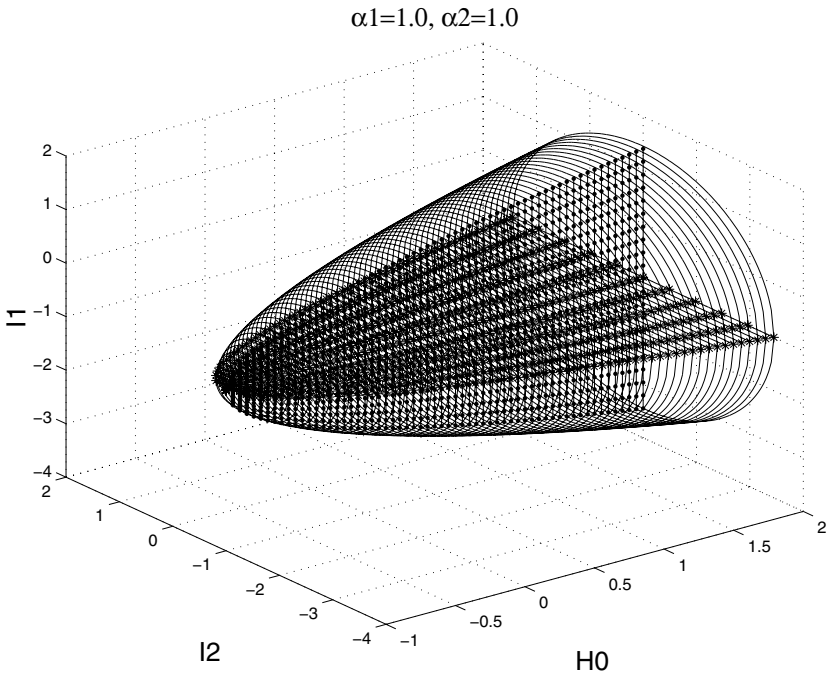

Figure 2. *EMBD of an a priori stable system.*

motion is allowed only for I values which are interior to this paraboloid notice that from (2.5)

$$0 \leq \frac{y^2}{2} + \frac{x^2}{2} + \frac{1}{8}\left(x^2+y^2\right)^2 = h - \frac{1}{2}\sum_{i=1}^{2}(I_i+\alpha_i)^2 + \frac{\alpha_1^2+\alpha_2^2}{2}.$$

The energy surfaces which appear as caps in the frequency space are "flattened" here to discs in the energy-momentum space. An example of an energy surface in the (I_2, I_1) plane, corresponding to the two dimensional (2D) slice of Figure 2 at $H_0 = 1$, is presented in Figure 3A. The thin vertical lines in the 2D sections of the EMBD indicate the region of allowed motion. In Figure 3B we present a 2D slice in the (H_0, I_1) plane at $I_2 = 0$, on which we schematically indicate the corresponding Fomenko graph by a thick black line. The Fomenko graph for any positive h and an interior I_2 value is simply a segment: each interior point on this segment corresponds to a single 3-torus, and each of the end points corresponds to a normally elliptic 2-torus ("atom A" in [18]). For such a fixed I_2 value the energy surface appears as a 2-sphere in the (x, y, I_1) space. The poles of this sphere are normally elliptic 2D tori, and they correspond to the boundaries of this component of the energy surface. Equivalently, we may think of a natural generalization of the Fomenko graphs to branched surfaces, and in this trivial case the branched surface is simply a single disk, as shown in Figure 9A: an interior point to the disc corresponds to a 3-torus, and a point on the disc boundary corresponds to a 2-torus.

The *strong resonances* $\omega_i = 0, i = 1, 2$, correspond here to the hyperplanes $I_i = -\alpha_i$.

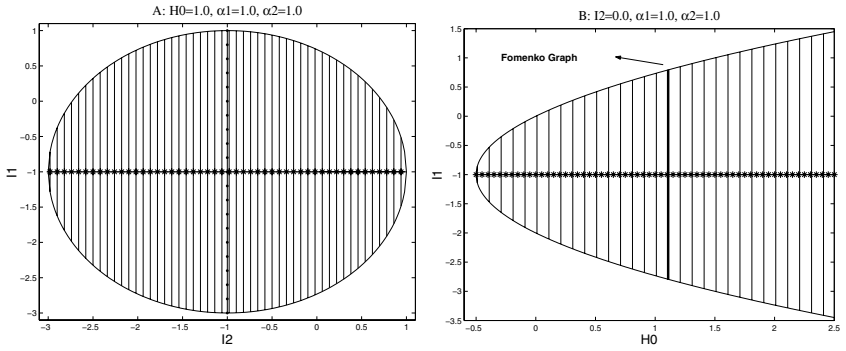

Figure 3. 2*D slices of an EMBD of an a priori stable system.* A: *One energy surface.* B: *Range of energy values for a fixed value of* I_2 *and a schematic Fomenko graph.*

Their intersections with the singularity manifold p^0_{ell} satisfy

$$\dot{\theta}_i = \left.\frac{\partial H}{\partial I_i}\right|_{x=y=0, I_i=-\alpha_i} = \left.\frac{dH(p^0_{ell})}{dI_i}\right|_{x=y=0, I_i=-\alpha_i} = 0.$$

Namely, it *corresponds to a fold in the singularity manifold* p^0_{ell}. Here the relation between total derivatives with respect to I_i along p^0_{ell} and the corresponding partial derivatives of H is trivial. Notice that the same relation is satisfied even when the location of the singularity manifold depends on I_i since $\nabla_{x,y}H$ vanishes on the singularity surfaces. This latter property is coordinate-independent as long as the coordinates are suitable.

In Figures 2 and 3 we indicate the strongest resonant 3-tori by starred lines (for $\dot{\theta}_1 = 0$) and dotted lines (for $\dot{\theta}_2 = 0$). The intersection of these surfaces (here planes) with the singularity surface ($x = y = 0$) corresponds to the strongly resonant families of lower dimensional tori $\{(x, y, I) = (0, 0, -\alpha_1, I_2)\}$,$\{(x, y, I) = (0, 0, I_1, -\alpha_2)\}$. These two families of 2-tori intersect at the minimal possible energy where $(I_1, I_2) = (-\alpha_1, -\alpha_2)$, corresponding to a 2-torus of fixed points. Namely, this torus of fixed points corresponds to a topological change in the energy surface—for energies below the value at which this torus appears there is no allowed motion. For energies above it we have one connected component of energy surface as described above. This observation is a trivial manifestation of Theorem 2.

5.3. Qualitative behavior of the near-integrable system (S). The motion in the near-integrable system $H(\theta, I) = H_{st}(I) + \varepsilon H_1(\theta, I)$ is restricted to the energy level $H = h$. Since $H_1(\theta, I)$ is assumed to be bounded, we obtain that the unperturbed energy surfaces with $H_{st}(I) = h^*$, $|h^* - h| < C\varepsilon$ supply an a priori bound to the motion. For energy surfaces of large extent, such an a priori bound is irrelevant due to Nehorošev-type theorems and the Arnold conjecture. Hence, in this case the only new information obtained from the EMBD is regarding the appearance of strong lower dimensional resonant tori (and even this information can be extracted from the frequency plot). Near the doubly resonant normally elliptic lower dimensional torus, where $(x, y, I) = (0, 0, -\alpha_1, -\alpha_2)$, one may expect small perturbations to produce large instabilities. Our trivial observation regarding the extent of the energy surface immediately shows that the extent of the instability cannot be larger than $O(\sqrt{\varepsilon})$, the extent

in the I space of the energy surfaces with $H_{st}(I) = h^*$, $|h^* - h| < C\varepsilon$. We may expect that the behavior near the doubly resonant torus will be dramatically different if the dependence on the actions is either linear or indefinite, e.g.,

$$H_{st-unbounded}(x, y, I_1, I_2) = \frac{y^2}{2} + \frac{x^2}{2} + \frac{1}{8}\left(x^2 + y^2\right)^2 + \alpha_1 I_1 + \alpha_2 I_2 - \frac{I_1^2}{2} + \frac{I_2^2}{2};$$

namely, the energy surfaces are unbounded, and, in particular, the energy surface passing through the elliptic double resonant fixed point is unbounded. Such considerations are the trivial analogues to the nonlinear stability theorems of Arnold–Marsden and have been studied and discussed in the context of normal forms near elliptic fixed points [2, 40].

6. A priori unstable systems. The phase space structure of the standard Hamiltonian H_{ust} (see (2.6)),

$$H_{ust}(x, y, I_1, I_2) = \frac{y^2}{2} - \frac{x^2}{2} + \frac{x^4}{4} + \frac{1}{2}\sum_{i=1}^{2}\left((\alpha_i + I_i)^2 - \alpha_i^2\right) \tag{6.1}$$

$$= H_{xy}(x, y) + H_I(I), \tag{6.2}$$

is given by the product of a figure eight motion in the xy plane and a family of 2-tori in the (θ, I) space. The precise structure of each energy surface, which demonstrates how a given energy may divide between the three modes (degrees of freedom) requires a bit more attention. Since there are no global action-angle coordinates in the (x, y) plane, it is instructive to start with the presentation of the energy surfaces in the energy-momentum space and then discuss the presentation in the frequency space.

6.1. Energy surfaces in the energy-momentum space (U). To construct the EMBD we find the singularity manifolds of the Hamiltonian (6.1). These manifolds correspond to fixed points of $H_{xy}(x, y)$. The normally elliptic singularity surfaces, corresponding to $\{x = \pm 1, y = 0\}$, are given by the identical[11] paraboloids

$$p_{ell}^{\pm}(h, I_1, I_2) = \left\{(h, I_1, I_2) \Big| \quad \frac{1}{2}\sum_{i=1}^{2}\left((\alpha_i + I_i)^2 - \alpha_i^2\right) = h + \frac{1}{4},\ h \geq h_{ell}\right\},$$

where

$$h_{ell} = -\frac{1}{4} - \frac{1}{2}\sum_{i=1}^{2}\alpha_i^2.$$

The normally hyperbolic singularity surface corresponding to $x = y = 0$ and its separatrices is given by the paraboloid

$$p_{hyp}^{0}(h, I_1, I_2) = \left\{(h, I_1, I_2) \Big| \quad \frac{1}{2}\sum_{i=1}^{2}\left((\alpha_i + I_i)^2 - \alpha_i^2\right) = h,\ h \geq h_{hyp}\right\},$$

[11] Adding an asymmetric term like ηx to H_{ust} lifts this degeneracy.

where

$$h_{hyp} = -\frac{1}{2}\sum_{i=1}^{2}\alpha_i^2.$$

In Figure 4 an EMBD of system (6.1) is presented as two nested paraboloids. The singularity manifolds are drawn according to the normal stability of the lower dimensional invariant tori they represent—the normally elliptic singularity manifolds ($p^{\pm}_{ell}(h, I_1, I_2)$) are drawn as a collection of solid curves, whereas the *normally hyperbolic* singularity manifold ($p^{0}_{hyp}(h, I_1, I_2)$) is drawn as a collection of black *dashed* curves. Thus we follow the traditional notation in bifurcation diagrams.

Given an energy surface $H_{ust}(x, y, I_1, I_2) = H_0 = h$ with $h_{ell} \le h < h_{hyp}$, the three dimensional (3D) and 2D EMBD look locally similar to those of the a priori stable system, presented in Figures 2 and 3: for each fixed energy value in this range the energy surface is a disk in the (I_2, I_1) plane. However, each point interior to this disk corresponds to *two* sets of 3-tori, one in each well of the potential of $H_{xy}(x, y)$. Points on the boundary of the disk correspond to the *two* normally elliptic 2-tori, $\{x = \pm 1, y = 0, H_{ust}(\pm 1, 0, I_1, I_2) = h\}$. Hence, the Fomenko graph for any one dimensional (1D) section of each such disk is given by two disconnected segments, as shown in Figure 5B. Equivalently, the generalized branched surfaces for this range of energies is the union of two disconnected discs (see Figure 9B). Each point belonging to the interior of the branched surfaces represents, as before, a single 3-torus, and every point on the solid boundary of the discs represents, as before, a single, normally elliptic 2-torus. The multiplicity in the number of components of the level set corresponding to a given (h, I_1, I_2) is expressed by the multiplicity in the number of components of the branched surfaces for these values of (h, I_1, I_2); see section 3.

For $h \ge h_{hyp}$ the energy surfaces include the singular level set of the separatrices, which divides the energy surface into two topologically different regimes; see Figure 5A. A point (h, I_1, I_2) inside the disk enclosed by $p^{0}_{hyp}(h, I_1, I_2)$ (the dashed circle in Figure 5A) corresponds to a single 3-torus. Trajectories belonging to this torus encircle both wells in the xy plane. A point inside the ring bounded between $p^{0}_{hyp}(h, I_1, I_2)$ and $p^{\pm}_{ell}(h, I_1, I_2)$ corresponds to *two* sets of 3-tori; trajectories belonging to one of these tori oscillate in one of the wells in the xy plane. The Fomenko graph for this case is shown schematically on the cross-section in Figure 5B (in thick black). The generalized branched surfaces here are two rings which are glued together in a central disk (Figure 9C). Each regular point of the branched surface corresponds to a single 3-torus, each point belonging to the dashed circle corresponds to a normally hyperbolic 2-torus and its separatrices, and each point belonging to the solid (outer) boundaries of the rings corresponds to a single normally elliptic 2-torus.

Intersections of the singularity manifolds with the hypersurfaces of strongest resonances correspond to folds of these singularity manifolds in the EMBD (see Figures 4 and 5). This is the essence of Theorem 1 (see section 8.1). For example, the paraboloids $p^{0}_{hyp}(h, I_1, I_2)$ and $p^{\pm}_{ell}(h, I_1, I_2)$ fold as they cross the surface $I_1 = -\alpha_1$ (and similarly at $I_2 = -\alpha_2$) and indeed $\dot{\theta}_i|_{p_f} = \alpha_i + I_i$. Thus, the families of 2-tori, $p^{\pm}_{ell}(h, -\alpha_1, I_2)$, $p^{\pm}_{ell}(h, I_1, -\alpha_2)$, $p^{0}_{hyp}(h, -\alpha_1, I_2)$, and $p^{0}_{hyp}(h, I_1, -\alpha_2)$, are all resonant and the 2-tori $p^{\pm}_{ell}(h_{ell}, -\alpha_1, -\alpha_2)$ and $p^{0}_{hyp}(h_{hyp}, -\alpha_1,$

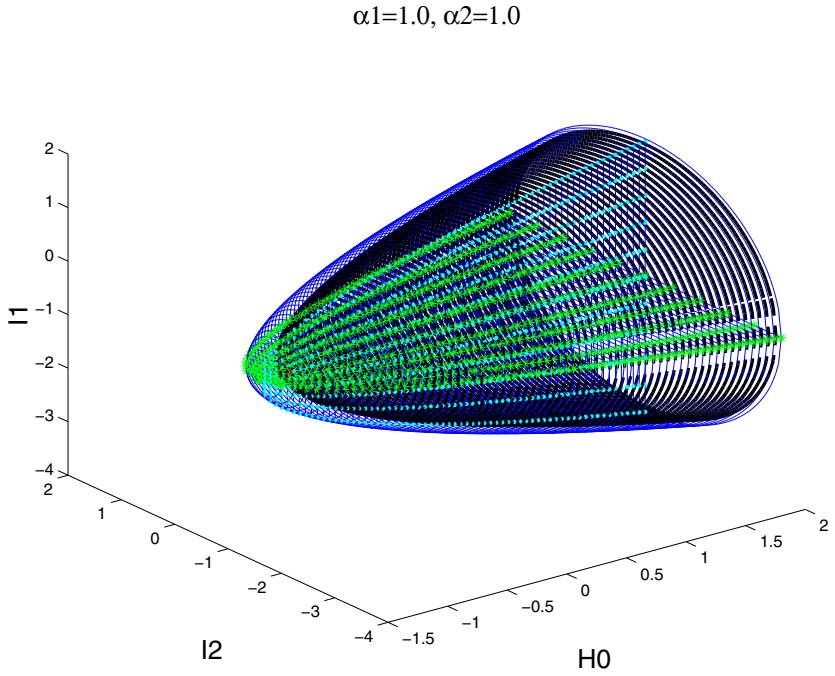

Figure 4. *EMBD of an a priori unstable system.*

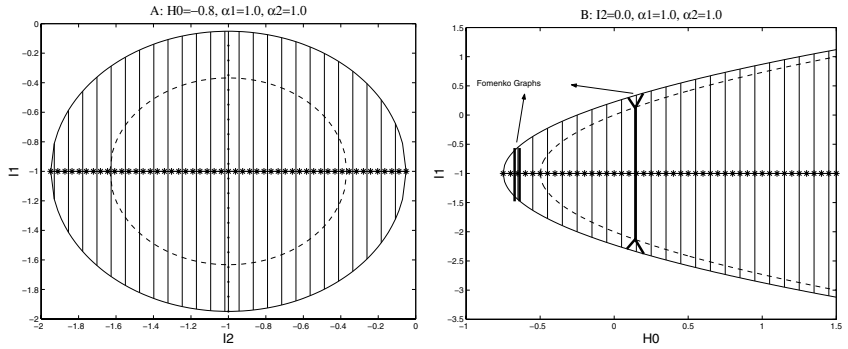

Figure 5. *2D slices of an EMBD of an a priori unstable system with $h > h_{hyp}$.* A: *One energy surface.* B: *Range of energy values for a fixed value of I_2 and a schematic Fomenko graph.*

$-\alpha_2$) are doubly resonant; these are 2-tori of fixed points. In Figure 4 the strong resonance in the I_1 direction ($\dot{\theta}_1 = 0$) is denoted by a surface of green starred lines and the strong resonance in the I_2 direction ($\dot{\theta}_2 = 0$) by a surface of cyan dotted lines; the *double fold* corresponding to a 2-resonant hyperbolic 2-torus (a hyperbolic torus of fixed points) is denoted by a red star.

Observe that the topology of the family of equi-energy normally hyperbolic lower dimensional tori ($p^0_{hyp}(h, \cdot)$, with fixed h) changes exactly at this double fold point, $p^0_{hyp}(h_{hyp}, -\alpha_1, -\alpha_2)$, where a 2-torus of fixed points resides; for $h < h_{hyp}$ the singularity surface $p^0_{hyp}(h, \cdot)$ does not exist and the energy surfaces have two disconnected components (Figure 9B), whereas for

$h > h_{hyp}$ the singularity surface $p^0_{hyp}(h,\cdot)$ is a circle and the two components of the energy surface connect on this circle (Figure 9C). This is again a manifestation of Theorem 2 (see section 8.1). Similarly, for the natural n DOF generalization of H_{ust},

$$H^n_{ust}(x,y,I_1,\dots,I_{n-1}) = \frac{y^2}{2} - \frac{x^2}{2} + \frac{x^4}{4} + \frac{1}{2}\sum_{i=1}^{n-1}\left((\alpha_i + I_i)^2 - \alpha_i^2\right) \tag{6.3}$$

$$= H_{xy}(x,y) + H^n_I(I), \tag{6.4}$$

$p^0_{hyp}(h,\cdot)$ changes from nonexistence for $h < h_{hyp}$ to an $n-2$ sphere for $h > h_{hyp}$. In particular, for $n = 2$, there are either none or two nonresonant hyperbolic circles on each energy surface. If the dependence on the I variables is indefinite, then one may have other topological changes in $p^0_{hyp}(h,\cdot)$ occurring at the $(n-1)$-resonant $(n-1)$-torus; either the genus of $p^0_{hyp}(h,\cdot)$ changes or two components of $p^0_{hyp}(h,\cdot)$ coalesce/separate. Notice that the flow along the lower dimensional $(n-1)$-torus reverses its direction as a strong resonance surface is crossed (namely, $\dot{\theta}_i|_{p_f}$ changes its sign there). This property holds for the general case of nonseparable systems as well (see [46, 38, 37]).

We emphasize that the appearance of an $n-1$ dimensional torus of fixed points which is normally hyperbolic is a persistent[12] phenomena in integrable n $(n \geq 2)$ DOF Hamiltonian systems [38] and is not related to the symmetric form of (6.3).

6.2. Energy surfaces in the frequency space (U). For small energy levels, $h_{ell} \leq h < h_{hyp}$, we have seen that the disk $H_{ust}(x,y,I_1,I_2) = h$ in the (I_2,I_1) plane (see Figures 5B and 9B) corresponds to two separate smooth compact components of the energy surface. In the frequency space these appear as one cap of hyperbola, centered at the origin. Indeed, the natural frequency in the xy plane at the elliptic points is $\omega_0(h,I_1,I_2)|_{p^{\pm}_{ell}(h,I_1,I_2)} = \sqrt{2}$, the direction of rotation is preserved for all orbits (so $\omega_0(h,I_1,I_2) \geq 0$), and the frequency monotonically decays as the action of the periodic orbits grows. Denoting by $\omega_{0\,\min}(h) > 0$ the frequency of the two symmetric periodic orbits in the xy plane satisfying $H_{xy}(x,y) = h$, it follows that for this range of energies

$$\omega_{0\,\min}(h) \leq \omega_0(h,I_1,I_2) \leq \sqrt{2}. \tag{6.5}$$

In Figure 6 an example of such a cap shaped energy surface of system (6.1) in the frequency space is shown.

For $h \geq h_{hyp}$ the behavior near the separatrices needs to be presented. Since the frequency in the xy plane is well defined for all orbits except the separatrices, and since $\omega_0(x,y) \to 0$ as the separatrix is approached, defining $\omega_0(0,0) = 0$ makes $\omega_0(x,y)$ a continuous (nondifferentiable) function of the xy energy level. (This observation is used extensively in the frequency map plots; see [28].) Hence, for $H_0 = h \geq h_{hyp}$, an energy surface in the frequency space has an annular cap component which meets at the (singular) circle $\omega_0 = 0$ a central cap;

[12] The existence of such a torus may be formulated as the existence of a transverse intersection of some finite dimensional manifolds. Hence, using the transversality theorem, one proves that it exists for a C^1-open set of integrable Hamiltonians, which we take hereafter as the definition of persistence.

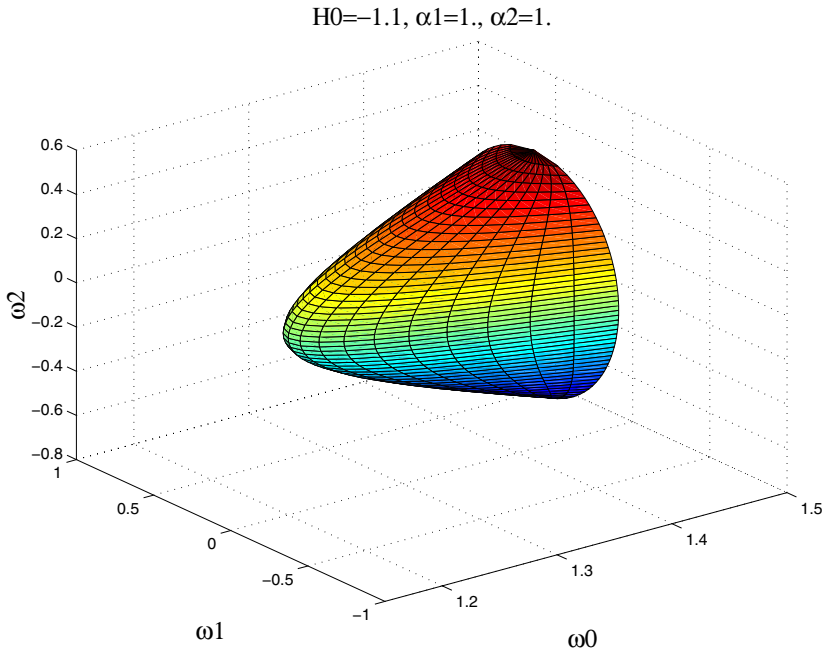

Figure 6. *Energy surface of an a priori unstable system in the frequency space for* $h_{ell} < H_0 < h_{hyp}$.

see Figure 7. The annular cap corresponds to the two sets of tori for which the motion is restricted to one of the wells in the xy plane, whereas the central cap corresponds to a single family of 3-tori for which the motion in the xy plane surrounds both wells of the potential. Recall that strong resonances are created when the energy surface intersects one of the $\omega_i = 0$ planes. However, here, the surface approaches the plane $\omega_0 = 0$ singularly, and the normally hyperbolic torus is not resonant in the θ_0 direction.

6.3. Qualitative behavior of the near-integrable system (U). Using the plots of the EMBD we may read off all possible sources of instabilities for near-integrable n DOF systems with unperturbed Hamiltonian of the form (6.3). Here we need to combine several effects:

- Instabilities associated with the regular resonance web. Such instabilities may appear near any point in the EMBD.
- Instabilities associated with splitting of the separatrices (as in 1.5 DOF systems). Such instabilities may appear for any $h > h_{hyp}$ in an ε neighborhood of the surface $p^0_{hyp}(h, \cdot)$.
- Instabilities associated with the existence of families of separatrices on the same energy surface (as in Arnold's conjecture for the existence of whiskered transition chain). For $n \geq 3$, these appear for any $h > h_{hyp}$ near the surface $p^0_{hyp}(h, \cdot)$.
- Instabilities associated with strongly resonant normally hyperbolic tori. For $k < n-1$, the k-resonant normally hyperbolic tori appear for all $h > h_{hyp}$, and their effect must be included in the above mentioned transition chain.
- Instabilities associated with the topological bifurcation of the energy surface near $h = h_{hyp}$. There, $p^0_{hyp}(\cdot)$ has an $n-1$ fold point and the normally hyperbolic torus $p^0_{hyp}(h_{hyp}, \cdot)$ is a torus of fixed points. Hence, these are the instabilities associated

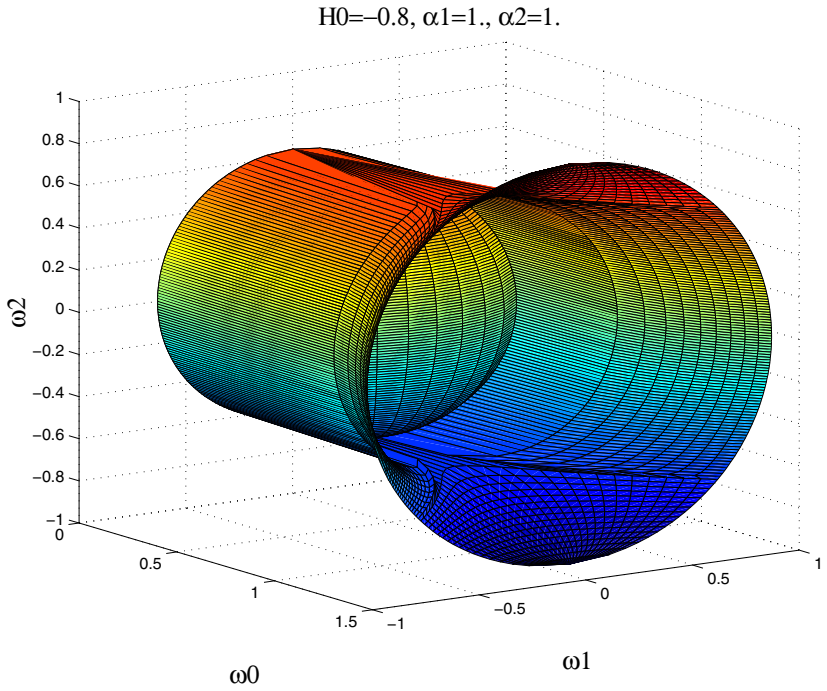

Figure 7. *Energy surface of an a priori unstable system in the frequency space for $H_0 > h_{hyp}$.*

with perturbations of a normally hyperbolic torus of fixed points in the nondegenerate case.

While the analysis of each of the above items is not yet well understood, we propose that the inclusion of rough lower bounds on the instability associated with each of the above phenomena supplies nontrivial information on the system. In Figure 8 we plot on a 2D slice of the EMBD and $O(\varepsilon)$ band around the separatrix level sets (the light shaded region), and indicate an $O(\varepsilon)$ slab of energies to which the perturbed motion is restricted near a hyperbolic resonance (the dark shaded strip). The geometry near the hyperbolic resonant tori immediately presents itself as a source for larger instabilities than the nonresonant terms. The analysis of this case for $n = 2$ has been developed; see [23] and references therein. Here we see that in the 3 DOF context the hyperbolic resonant 2-tori, $p_{hyp}(h, -\alpha_1, I_2(h))$ and $p_{hyp}(h, I_1(h), -\alpha_2)$, belong to the circle of equi-energy normally hyperbolic 2-tori, $p_{hyp}(h, \cdot)$; hence, one is lead to the study of whiskered transition chains with resonant gaps (see [9] and references therein). The subject of transition chains of whiskers in a priori unstable systems has received much attention in recent years (see, e.g., [8, 49, 50] and references therein). Furthermore, as $(I_1, I_2) \to (-\alpha_1, -\alpha_2)$ we approach a double resonant hyperbolic torus—in this case the 3D figure corresponds to a revolution of the EMBD in Figure 8 around the starred line, with the strong resonant planes intersecting as in Figure 4. Here the radius (in I) of the circle $p_{hyp}(h, \cdot)$ scales as $\sqrt{\varepsilon}$ (see Figure 8); hence the transition chain created near such a double resonant hyperbolic torus cannot create large instabilities. If the terms in I are indefinite near such a torus, this situation may change (though our preliminary numerical

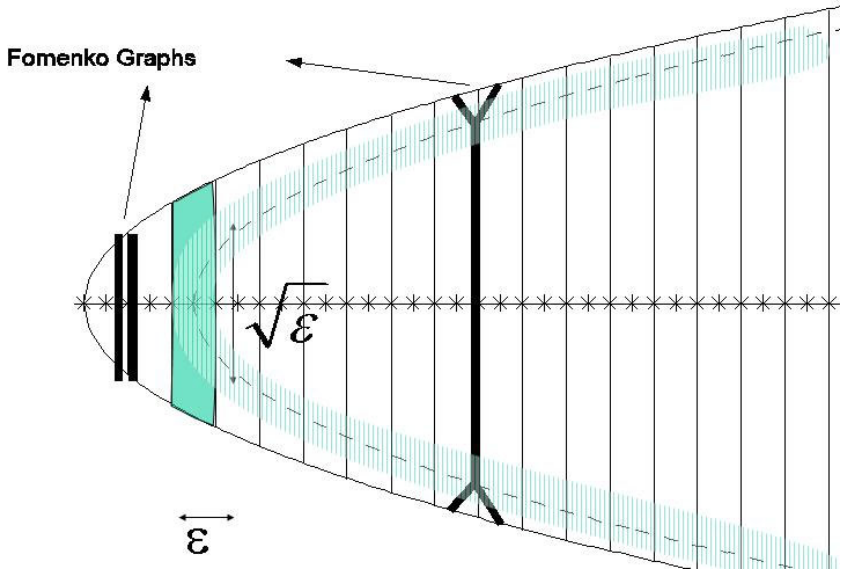

Figure 8. *2D slice of the EMBD of the perturbed motion. Shaded strip: Region of allowed motion for perturbed orbits near hyperbolic resonance. Dashed region: Homoclinic chaos region.*

simulations appear to indicate that even then the instability induced by the separatrices is not significantly enhanced [38]).

Finally, we note that the doubly resonant elliptic tori $p^{\pm}_{ell}(h, -\alpha_1, -\alpha_2)$ reside on two small separate components of the energy surface and hence cannot induce large instabilities, and that other cases corresponding to unbounded energy surfaces may be classified similarly.

7. Bifurcating systems. For n DOF systems with $n \geq 3$ the appearance of parabolic resonant tori is persistent (see [38]); hence their study is both mathematically fascinating and physically relevant. Combining our understanding of the stable and unstable systems, we can now study H_{bif}:

$$H_{bif}(x, y, I_1, I_2) = \frac{y^2}{2} - \frac{x^2}{2} I_1 + \frac{x^4}{4} + \left(\mu_1 + \frac{1}{2}\right) \frac{I_1^2}{2} + \frac{I_2^2}{2} + \alpha_2 I_2 + \alpha_3 I_1 I_2. \tag{7.1}$$

The phase space structure of the Hamiltonian H_{bif} for any fixed I is obvious; for $I_1 > 0$ it is given by the product of a figure eight motion in the xy plane and a family of 2-tori in the (θ, I) space as in H_{ust}, whereas for $I_1 < 0$ it corresponds to an elliptic motion around the origin in the xy plane and a family of 2-tori in the (θ, I) space as in H_{st}. At $I_1 = x = y = 0$ the system has a family of normally parabolic 2-tori. To understand the precise structure of each energy surface, we again construct the EMBD and the corresponding branched surfaces and then present the interesting energy surfaces in the frequency space.

The symmetric form of (7.1) implies that at $I_1 = 0$ we have a pitchfork bifurcation in the xy plane, whereas for a generic asymmetric integrable bifurcating Hamiltonian one should consider instead a saddle-center bifurcation at $I_1 = 0$. The EMBD and branched surfaces

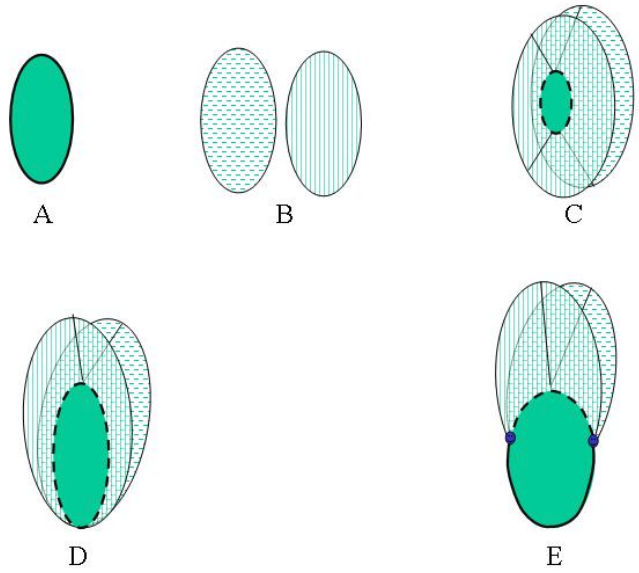

Figure 9. *Generalized Fomenko graphs: The branched surfaces.*

analysis of such systems is analogous to the one presented here. The phenomena of parabolic resonances (PR) in the asymmetric case has not been investigated yet.

7.1. Energy surfaces in the energy-momentum space (B). Recall that the boundary of the allowed region of motion is composed of the singularity surfaces corresponding to lower dimensional normally elliptic tori. For (7.1), these are given by the normally elliptic tori at $\{(x,y)=(\pm\sqrt{I_1},0);\ I_1>0\}$,

$$p^{\pm}_{ell}(h,I_1,I_2)=\left\{(h,I_1,I_2)|\ \mu_1\frac{I_1^2}{2}+\frac{I_2^2}{2}+\alpha_2 I_2+\alpha_3 I_1 I_2=h;\ h\geq h^{+}_{\min},I_1>0\right\}, \tag{7.2}$$

and the elliptic tori at $\{(x,y)=(0,0);\ I_1<0\}$,

$$p^{0}_{ell}(h,I_1,I_2)=\left\{(h,I_1,I_2)\ |\ \left(\mu_1+\frac{1}{2}\right)\frac{I_1^2}{2}+\frac{I_2^2}{2}+\alpha_2 I_2+\alpha_3 I_1 I_2=h;\ h\geq h^{0}_{\min},I_1<0\right\}. \tag{7.3}$$

Another surface of singularity on which the hyperbolic tori $\{(x,y)=(0,0);\ I_1>0\}$ and their separatrices live is given by

$$p^{0}_{hyp}(h,I_1,I_2)=\left\{(h,I_1,I_2)\ |\ \left(\mu_1+\frac{1}{2}\right)\frac{I_1^2}{2}+\frac{I_2^2}{2}+\alpha_2 I_2+\alpha_3 I_1 I_2=h;\ h\geq h^{0}_{\min},I_1>0\right\}. \tag{7.4}$$

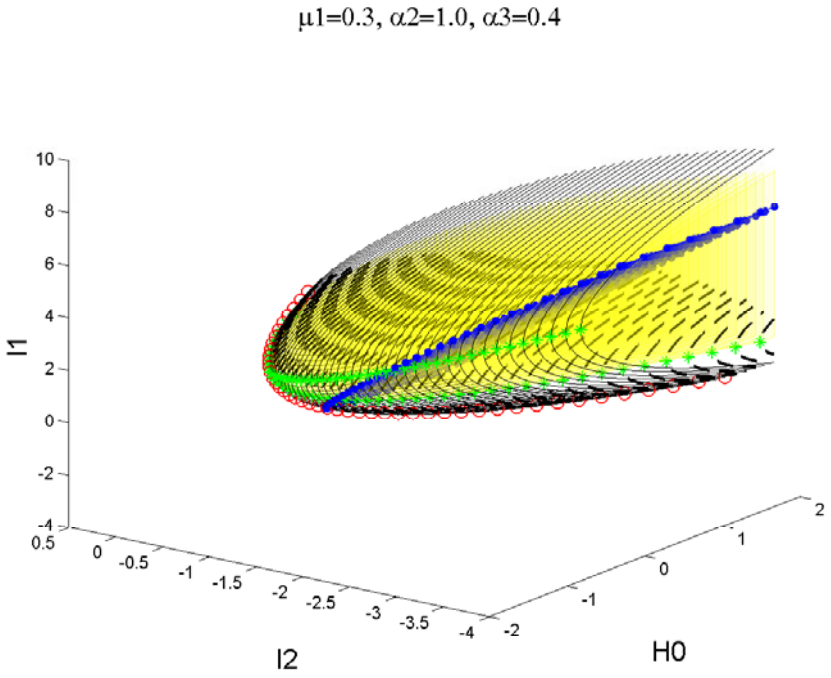

Figure 10. *EMBD for the bifurcating Hamiltonian, H_{bif}.*

Expressing the Hamiltonian on these surfaces in a quadratic form,

$$H_{bif}(0,0,I_1,I_2) = \frac{1}{2}\left(\mu_1 + \frac{1}{2} - \alpha_3^2\right)\left(I_1 - \frac{\alpha_2\alpha_3}{\mu_1 + \frac{1}{2} - \alpha_3^2}\right)^2 + \frac{1}{2}\left(I_2 + \alpha_2 + \alpha_3 I_1\right)^2 - \frac{1}{2}\alpha_2^2 - \frac{1}{2}\frac{(\alpha_2\alpha_3)^2}{\mu_1 + \frac{1}{2} - \alpha_3^2}, \tag{7.5}$$

$$H_{bif}(\pm\sqrt{I_1},0,I_1,I_2) = \frac{1}{2}(\mu_1 - \alpha_3^2)\left(I_1 - \frac{\alpha_2\alpha_3}{\mu_1 - \alpha_3^2}\right)^2 + \frac{1}{2}\left(I_2 + \alpha_2 + \alpha_3 I_1\right)^2 - \frac{1}{2}\alpha_2^2 - \frac{1}{2}\frac{(\alpha_2\alpha_3)^2}{\mu_1 - \alpha_3^2}, \tag{7.6}$$

shows that the sign of $\mu_1 - \alpha_3^2$ determines whether the energy surfaces are bounded in I. Here, for simplicity, we present a bounded case:

$$\mu_1 - \alpha_3^2 > 0, \qquad \alpha_2 > 0, \qquad 0 < \alpha_3 < 1. \tag{7.7}$$

Other cases change some of the inequalities below, leading to a different EMBD and may be similarly analyzed; see [36, 35, 37, 38], where we considered mainly unbounded models. Here, (7.5) and (7.6) define paraboloids, and their intersections with the plane of constant energy define ellipses (see Figures 10, 11, 12, 13, 14, 15, 16).

The minimal energies for which these paraboloids are defined are

$$h^{+}_{\min} = -\frac{1}{2}\alpha_2^2 - \frac{1}{2}\frac{(\alpha_2\alpha_3)^2}{\mu_1 - \alpha_3^2} < h^{0}_{\min} = -\frac{1}{2}\alpha_2^2 - \frac{1}{2}\frac{(\alpha_2\alpha_3)^2}{\mu_1 + \frac{1}{2} - \alpha_3^2}, \tag{7.8}$$

with the corresponding minimizing actions

$$(I_1, I_2)_{\min 0} = \left(\frac{\alpha_2\alpha_3}{\mu_1 + \frac{1}{2} - \alpha_3^2}, -\frac{\alpha_2\left(\mu_1 + \frac{1}{2}\right)}{\mu_1 + \frac{1}{2} - \alpha_3^2}\right),$$
$$(I_1, I_2)_{\min +} = \left(\frac{\alpha_2\alpha_3}{\mu_1 - \alpha_3^2}, -\frac{\alpha_2\mu_1}{\mu_1 - \alpha_3^2}\right).$$

Finally, notice that the surface $I_1 = 0$ cuts the paraboloids $p^{\pm}_{ell}(h, I_1, I_2)$ and $p^{0}_{ell,hyp}(h, I_1, I_2)$ along a parabola which corresponds to a family of normally parabolic 2-tori,

$$p^{0}_{par}(h, I_1, I_2) = \left\{(h, I_1, I_2) \mid I_1 = 0, \quad \frac{I_2^2}{2} + \alpha_2 I_2 = h, \ h \geq h^{p}_{\min}\right\}, \tag{7.9}$$

where

$$h^{p}_{\min} = -\frac{1}{2}\alpha_2^2 > h^{0}_{\min}.$$

From these computations we can already conclude that for the chosen set of parameters the energy surface's structure is represented by the branched surfaces shown in Figures 11B–E. Before describing the properties of these surfaces in detail, we examine the appearance of strong resonances so that the topological bifurcations and the appearance of resonant tori may be explicitly related.

Since

$$\omega_2(I_1, I_2) = \frac{\partial H_{bif}(x, y, I_1, I_2)}{\partial I_2} = I_2 + \alpha_2 + \alpha_3 I_1, \tag{7.10}$$

resonances in θ_2 (i.e., resonances in the direction of I_2) are given by the intersection of the domain of allowed motion with the plane

$$I_{2res} = -\alpha_2 - \alpha_3 I_1. \tag{7.11}$$

In particular, resonant lower dimensional tori appear when this plane intersects the paraboloids $p^{0}_{hyp}(h, \cdot)$, $p^{0}_{ell}(h, \cdot)$, $p^{\pm}_{ell}(h, \cdot)$, and $p^{0}_{par}(h, \cdot)$.

Due to the cross term $\frac{x^2}{2} I_1$ in H_{bif} (see (7.1)) we cannot get such a simple and explicit expression for the θ_1-resonant tori surface $\omega_1(I_1, I_2) = 0$. However, the intersection of this surface with the singularity surfaces may be easily found; the hyperbolic (resp., elliptic) lower dimensional tori $p^{0}_{hyp}(h, \cdot)$ (resp., $p^{0}_{ell}(h, \cdot)$) are resonant when $\omega_1^0 = 0$, where

$$\omega_1^0 = \frac{\partial H_{bif}(0, 0, I_1, I_2)}{\partial I_1} = \left(\mu_1 + \frac{1}{2}\right) I_1 + \alpha_3 I_2, \tag{7.12}$$

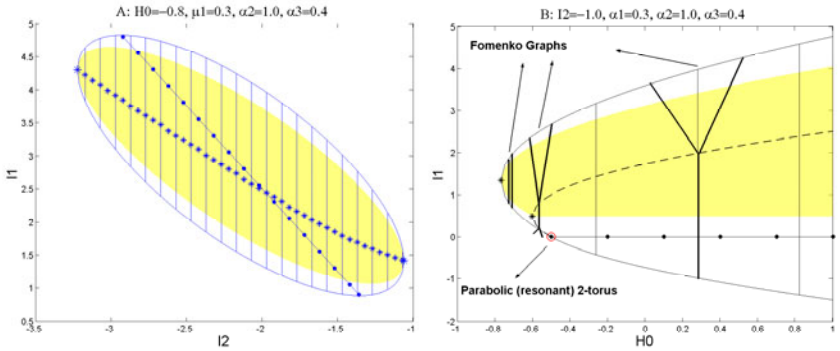

Figure 11. *2D slices of the EMBD of the bifurcating system, H_{bif}.* A: *An energy surface in the energy range $h^{\pm}_{\min} < H_0 < h^{0}_{\min}$.* B: *An interval of energy values for a fixed value of $I_2 = -\alpha_2$ and all three possible types of (schematic) Fomenko graphs for H_{bif}.*

so resonance occurs exactly at the fold of the singularity surface in the I_1 direction. Hence, the intersection of the plane

$$I_{1res0} = -\frac{\alpha_3}{\mu_1 + \frac{1}{2}} I_2$$

with the paraboloid $p^0_{hyp}(h,\cdot) \cup p^0_{par}(h,\cdot) \cup p^0_{ell}(h,\cdot)$ corresponds to the family of lower dimensional tori that are resonant in the I_1-direction (the green starred curves in Figure 10), $p^0_{res-1}(h,I)$. These tori are normally hyperbolic for $I_{1res} > 0$, normally elliptic for $I_{1res} < 0$, and, at $H_{bif} = h_{par-res1} = 0$, normally parabolic (then $I_{1res} = I_2 = 0$). Similarly, the elliptic lower dimensional tori at $(x,y) = (\pm\sqrt{I_1}, 0)$, $p^{\pm}_{ell}$, are θ_1-resonant when $\omega^{\pm}_1 = 0$, where

$$\omega^{\pm}_1 = \frac{\partial H_{bif}(\pm\sqrt{I_1}, 0, I_1, I_2)}{\partial I_1} = \mu_1 I_1 + \alpha_3 I_2.$$

Hence, the intersection of the plane

$$I_{1res\pm} = -\frac{\alpha_3}{\mu_1} I_2$$

with the paraboloids $p^{\pm}_{ell}(h, I_1, I_2)$ corresponds to these two families of normally elliptic lower dimensional tori that are resonant in the I_1-direction, $p^{\pm}_{res-1}(h,I)$ (denoted by green starred curves in Figure 10 as well). The manifold of 3-tori, which are strongly resonant in θ_1, $p_{res-1}(h, I_1, I_2)$, intersects the paraboloids $p^0_{hyp}(h,\cdot) \cup p^0_{par}(h,\cdot) \cup p^0_{ell}(h,\cdot)$ and $p^{\pm}_{ell}(h, I_1, I_2)$ along the families $p^0_{res-1}(h,I)$ and $p^{\pm}_{res-1}(h,I)$.

Clearly, from the form of (7.1), strong resonance in the xy plane (namely, the normal frequency $\Omega = \omega_0(h, I_1, I_2) = 0$) may occur only at the parabolic tori $p^0_{par}(h,0,I_2) = p^0_{hyp}(h,0,I_2) = p^{\pm}_{ell}(h,0,I_2)$, where $\omega^{\pm}_0 = \sqrt{2I_1}$ and $\omega^0_0 = \sqrt{-I_1}$ vanish. Notice that here, at $I_1 = 0$, the natural frequency of the lower dimensional torus does vanish, as opposed to the formal definition of vanishing ω^0_0 which we had introduced for $I_1 > 0$.

In Figure 10 a 3D EMBD of the system (7.1) (Hamiltonian H_{bif}) is presented for typical parameter values ($\mu_1 = 0.3$, $\alpha_2 = 1$, $\alpha_3 = 0.4$ in all the EMBD plots, and the corresponding

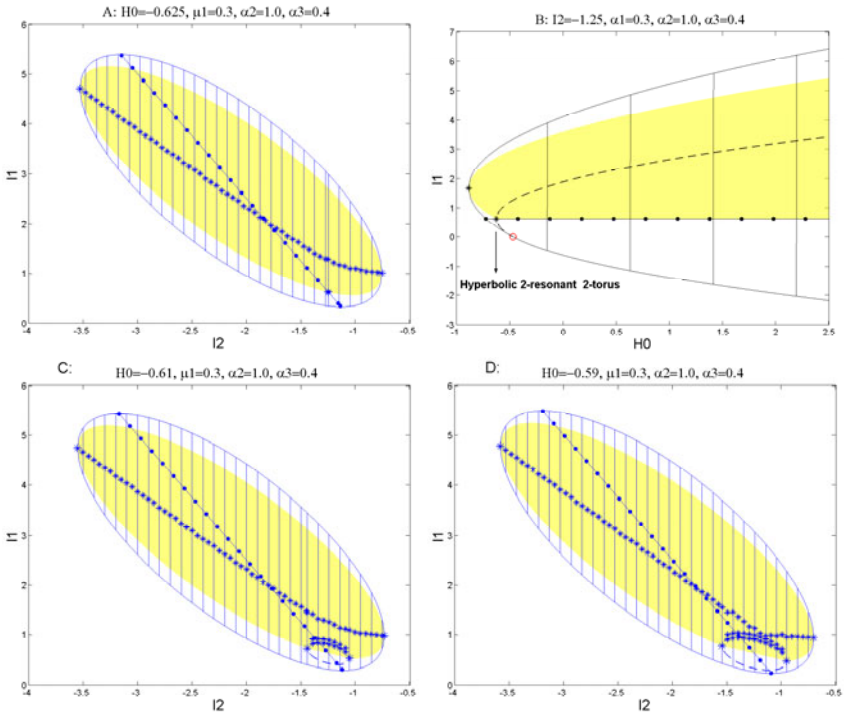

Figure 12. *2D slices of EMBD showing the energy range* $h^0_{\min} \le H_0 < h^0_p$. A: *An energy surface corresponding to the energy value* $H_0 = h^0_{\min}$, *showing the hyperbolic bifurcation point.* B: *A range of energy values which includes the bifurcation value at which a hyperbolic double resonance occurs for a fixed value of* $I_2 = I_{2\min 0}$. C, D: *Energy surfaces containing the singular ellipse (dashed line) corresponding to hyperbolic 2-tori and their separatrices.*

energy bifurcation values are $h^+_{\min} \approx -1.0714$, $h^0_{\min} = -0.625$, $h^p_{\min} = -0.5$, and $h_{par-res1} = 0$). The plot includes a limited set of I_2 values to allow a glimpse into its complicated inner structure: the manifold of solid curves corresponds to the singularity manifold of elliptic 2-tori, $p^{\pm}_{ell}(h, I_1, I_2)$ and $p^0_{ell}(h, I_1, I_2)$, the manifold of dashed curves to hyperbolic 2-tori, $p^0_{hyp}(h, I_1, I_2)$, and the curve of red circles to parabolic 2-tori, $p^0_{par}(h, I_1, I_2)$; the strongest resonance in the I_2-direction ($\dot{\theta_2} = 0$) is denoted by a blue surface of dotted lines and the 2-tori with the strongest resonance in the I_1-direction ($\langle\dot{\theta_1}\rangle_{xy} = 0$) by green starred curves. The yellow volume (or shaded regions in the 2D EMBD) corresponds to regular 3-tori on which $\dot{\theta_1}$ changes sign (back-flow). The surface of 3-tori which have strong resonance in the I_1-direction is contained in this region.

Taking the 2D slices $H_0 = h$ of Figure 10 for increasing h values, we describe below the structure of the corresponding branched surfaces in Figures 9B–E. The intersections of the strong resonance surfaces $\dot{\theta_2} = 0$ and $\omega_1(I_1, I_2) = 0$ with these 2D slices are denoted by a dotted line and a starred curve (which is calculated numerically), respectively.

For energies in the range $H_0 = h$, $h^+_{\min} \le h < h^0_{\min}$, the energy surfaces are composed of two separate components corresponding to oscillations in each of the potential wells (as in the low energy a priori unstable case). The energy surface in the EMBD is an ellipse, so

any 2D section of Figure 10 for this range of energies is similar to the EMBD slices of system H_{st} presented in Figure 3; see Figure 11A. The Fomenko graph for any 1D section of this ellipse is simply two segments; see Figure 11B. Equivalently, the branched surfaces are two identical discs as in Figure 9B, and the strong resonance surfaces $\omega_1(I_1, I_2) = \omega_2(I_1, I_2) = 0$ intersect the energy surface transversely, as shown by the starred and dotted lines in Figure 11A and schematically in Figure 14A. In particular, since the two resonant in the I_1 direction lower dimensional elliptic tori, $p^{\pm}_{res-1}(h, I_1, I_2)$, are separated along the circle $p^{\pm}_{ell}(h, I_1, I_2)$ by the two resonant in the I_2 direction lower dimensional elliptic tori, $p^{\pm}_{res-2}(h, I_1, I_2)$, it follows that the curves $p_{res-1}(h, I_1, I_2)$ and $p_{res-2}(h, I_1, I_2)$ of resonant 3-tori must intersect *at least* once in a double resonant 3-torus as shown schematically in Figure 14A; indeed, a transverse intersection of the strongest resonance curves is depicted in Figure 11A.

At $H_0 = h = h^0_{\min}$ (Figure 12A) a hyperbolic resonant bifurcation occurs; the singularity surface $p^0_{hyp}(h, I_1, I_2)$ appears in a 2-fold (since $I_{1\min 0} > 0$), creating a torus of fixed points which is normally hyperbolic; see Figure 12B, where the 2D slice $I_2 = I_{2\min 0}$ of Figure 10 is presented, and the newly born 2-resonant hyperbolic torus appears there in the fold of the dashed curve. Figure 12A shows that this torus does not appear at the intersection of the two strong resonance curves $\omega_1 = \omega_2 = 0$ (as in the a priori unstable case and as depicted schematically in Figure 14B). It appears as an isolated star[13] ($\dot\theta_1 = \omega^0_1 = 0$) residing on the dotted line ($\dot\theta_2 = \omega_2 = 0$). Topologically, at this point the two disks of the branched surfaces meet, so that for $H_0 = h$, $h^0_{\min} < h < h^p_{\min}$, we have, as before, a ring of I values for which two families of 3-tori, corresponding to oscillation in the wells, coexist and a central disk of I values for which only one family of 3-tori, corresponding to motion around the two wells, exists. The boundary between these regions is an ellipse of I values, corresponding to normally hyperbolic 2-tori; see Figures 12C,D and the corresponding Figures 9C and 5A.

Using the computation of $p^0_{res-1,2}(h, I)$, the *minimal number* of intersections of the strong resonance curves $p_{res-1}(h, I_1, I_2)$ and $p_{res-2}(h, I_1, I_2)$ in the interior disk is found to be one, as shown in Figure 14C. The 2D sections of Figure 10 for these ranges of energies demonstrate that for the bifurcating system (7.1) additional intersections appear[14] (see Figure 12A,C,D). A bifurcation in the iso-energetic strong resonance curve $\omega_1 = 0$ occurs at $H_0 = h = h^0_{\min}$. For $h < h^0_{\min}$ this resonance curve has one component and it is smooth; at the bifurcation point $h = h^0_{\min}$ it splits to two components—a smooth curve of resonant 3-tori with two resonant elliptic 2-tori at its boundary and a resonant hyperbolic 2-torus as a separate component (see Figure 12A). For $h^0_{\min} < h < h^c_{\omega_1}$, the iso-energetic curve $\omega_1 = 0$ has three components: the smooth component of resonant 3-tori with elliptic resonant 2-tori as its boundary and the other two components, which reside above and below the ellipse of hyperbolic 2-tori and meet at the two resonant hyperbolic 2-tori, as seen in Figure 12B. As the energy value increases, the components of $\omega_1 = 0$ approach each other until at the next bifurcation point of this curve, $H_0 = h = h^c_{\omega_1}$, all three components meet again (for the parameters chosen here $h^c_{\omega_1} \approx -0.59$; see Figure 12D), forming, for $h > h^c_{\omega_1}$, one nonsmooth component with cusp points at the resonant hyperbolic 2-tori, as seen in Figure 13A. (So the resonant surface $\omega_1 = 0$ folds in the shape of a nose looking toward the negative h values in the EMBD.)

[13] Look *below* the starred curve, at the boundary of the yellow shaded region.

[14] One can argue that this more complicated scenario is the generic one.

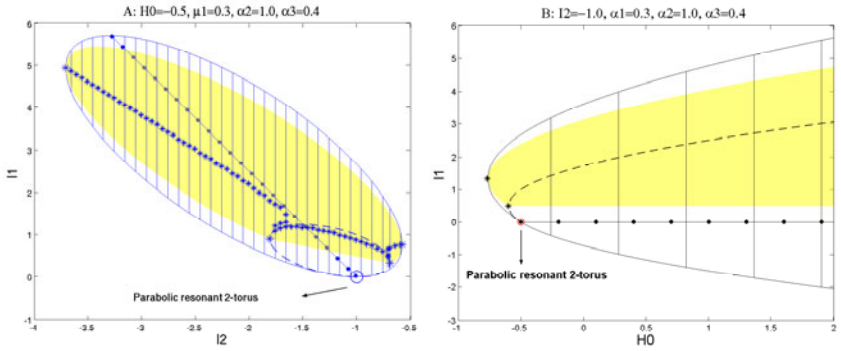

Figure 13. *2D slices of EMBD of the bifurcating system, H_{bif}, showing the parabolic bifurcation point.* A: *An energy surface corresponding to the energy value $H_0 = h^p_{\min}$.* B: *A range of energy values which includes the bifurcation value $H_0 = h^p_{\min}$ for a fixed value of $I_2 = -\alpha_2$.*

At $H_0 = h = h^p_{\min}$ the ellipses $p^0_{hyp}(h^p_{\min}, \cdot)$ and $p^{\pm}_{ell}(h^p_{\min}, \cdot)$ touch the $I_1 = 0$ plane at $I_2 = -\alpha_2$, creating a parabolic torus (see Figure 13A and the schematic representation of Figure 9D). This bifurcation is, again, associated with a fold in the singularity surfaces of the EMBD and therefore with a resonance of a lower dimensional torus (see Theorems 4 and 5 in section 8.2). Indeed, at $H_0 = h^p_{\min}$, the parabola $p^0_{par}(h, I_1, I_2)$ folds in the I_2 direction at $I_2 = -\alpha_2$; hence this parabolic 2-torus is resonant in θ_2:

$$\dot{\theta}_2\Big|_{(0,0,0,-\alpha_2)} = \frac{\partial H_{bif}(0,0,0,I_2)}{\partial I_2}\Big|_{I_2=-\alpha_2} = 0.$$

Furthermore, parabolicity of this torus implies that the torus is strongly resonant in the xy plane; namely, $\omega^0_0 = 0$, so at $h = h^p_{\min}$ a double resonance occurs at the torus $(x, y, I) = (0, 0, 0, -\alpha_2)$. This coincidence of resonances and of topological changes in the energy surfaces is shown schematically in Figures 14C–E. Figures 12 and 13 demonstrate its occurrence for (7.1). The dotted line, representing resonant tori in the I_2-direction, intersects the boundary of the allowed region of motion at the parabolic torus (a circle in the figure).

For $h > h^p_{\min}$, the branched surface is a disk with two flaps emanating from it (see Figure 9E), where the two end points of the flaps correspond to parabolic tori. For Hamiltonian (7.1), the ellipse $H_{bif}(0, 0, I_1, I_2) = h$ defines the boundary of this disc. The ellipse corresponds to hyperbolic tori for $I_1 > 0$ (the dashed part of the inner ellipses in Figure 15) and elliptic tori for $I_1 < 0$ (the lower solid part of the ellipses in Figure 15). The flaps' upper boundaries (upper solid line in Figure 15) are defined by the ellipse $H_{bif}(\pm\sqrt{I_1}, 0, I_1, I_2) = h$ for $I_1 \geq 0$. The two meeting points of the flaps (denoted by circles) with this disk correspond to the two parabolic tori which reside on the energy surface (see (7.9)).

Now, consider the relative location of the resonant in the I_1-direction 2-tori, $p^0_{res-1}(h, I)$, and the parabolic 2-tori, $p^0_{par}(h, I)$, on the ellipse $H_{bif}(0, 0, I_1, I_2) = h$. For h values which are slightly larger than $h^p_{\min}$, this pair of resonant 2-tori lives on the upper part of the ellipse, above the parabolic tori; hence they correspond to normally hyperbolic resonant 2-tori, as shown schematically in Figure 14D. For such values of h the curve $p_{res-1}(h, I_1, I_2)$ intersects only the upper part of the ellipse (the dashed part of the ellipse in Figure 15A, corresponding

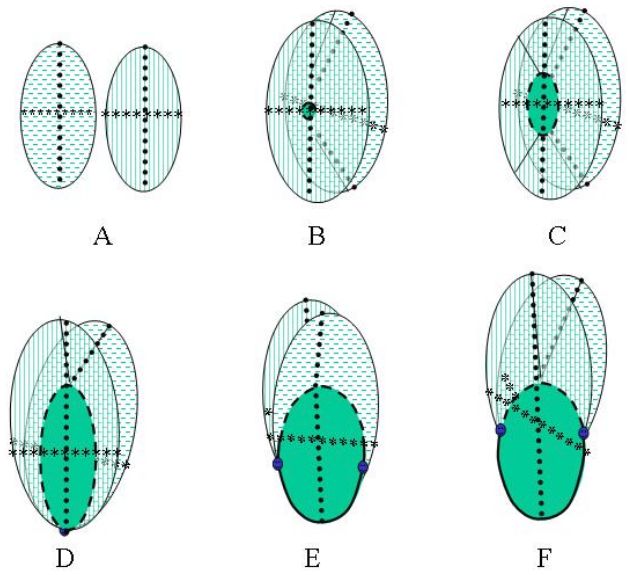

Figure 14. *Energy branched surfaces and strong resonance curves.*

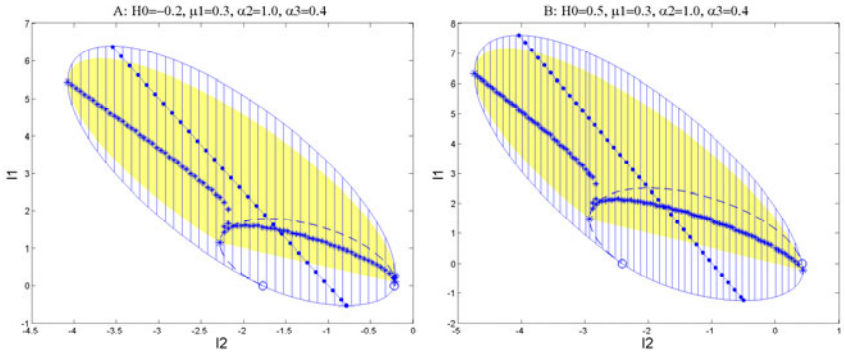

Figure 15. *2D slices of an EMBD of the bifurcating system, H_{bif}.* A: *An energy surface with $h^p_{\min} < H_0 < h_{par-res1}$.* B: *An energy surface with $H_0 > h_{par-res1}$.*

to hyperbolic tori), so there are no resonant in the I_1 direction normally elliptic 2-tori at the origin (i.e., $p^0_{hyp}(h, I_1, I_2) \cap p_{res-1}(h, I_1, I_2) = \varnothing$), as shown in Figure 15A. For energy values greater than $H_0 = h_{par-res1} = 0$ (i.e., for $h > h_{par-res1}$), this situation changes; for $H_0 = h > h_{par-res1}$, the resonant plane $p_{res-1}(h, I_1, I_2)$ intersects each of the curves $p^0_{hyp}(h, \cdot)$ and $p^0_{ell}(h, \cdot)$ at one point (see the schematic Figure 14F and the energy surface in Figure 15B). Namely, one of the resonant hyperbolic lower dimensional tori becomes normally elliptic for $H_0 = h > h_{par-res1}$. Therefore, at the bifurcation value, $H_0 = h_{par-res1} = 0$, the resonant plane in the I_1-direction intersects the ellipse $p^0_{hyp}(h, \cdot) \cup p^0_{par}(h, \cdot) \cup p^0_{ell}(h, \cdot)$ at $I_1 = I_2 = 0$, where a parabolic, resonant in the I_1 direction, lower dimensional torus is created (the schematic Figures 14E,F show the aforementioned intersections before and after

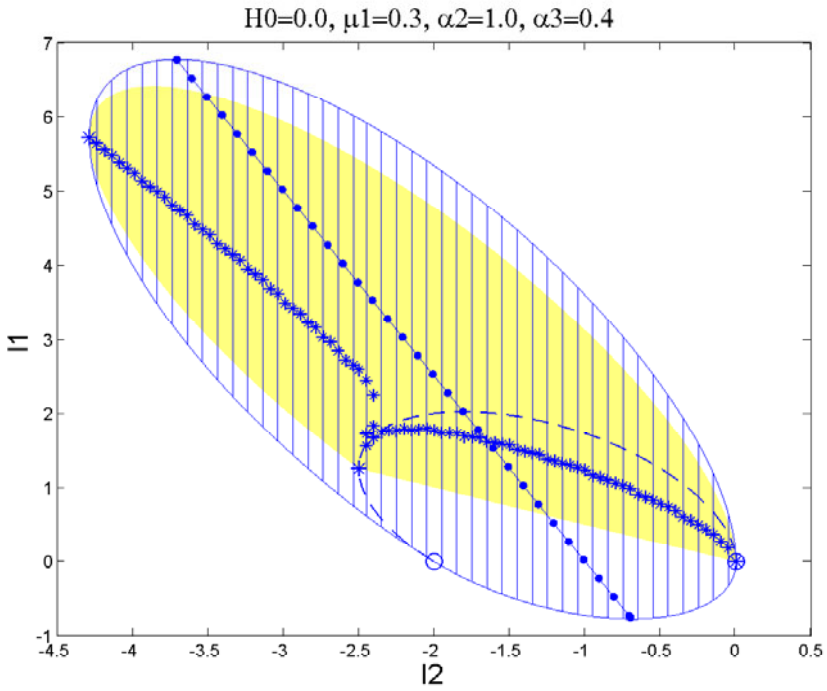

Figure 16. *A 2D slice of EMBD of the bifurcating system, H_{bif}. An energy surface with $H_0 = h_{par-res1}$, containing a strongly resonant in the I_1-direction parabolic 2-torus.*

this bifurcation). Indeed, Figure 16 shows that at $H_0 = h_{par-res1} = 0$ one of the resonant hyperbolic tori changes its stability and becomes parabolic. (The end point of the starred curve, $\omega_1 = 0$, intersects one of the circles denoting a parabolic 2-torus; note that at the bifurcation point $H_0 = h_{par-res1}$, the iso-energetic curve $\omega_1 = 0$ ceases to have two cusp points and thereon has only one cusp point at the remaining resonant hyperbolic 2-torus.) Figure 17A demonstrates that the resonance in the I_1-direction is indeed associated with a fold of the parabola $p^0_{hyp}(h, I_1, 0) \cup p^0_{par}(h, I_1, 0) \cup p^0_{ell}(h, I_1, 0)$ at the origin; the 2D slice of the EMBD at $I_2 = 0$ shows that the circle denoting the parabolic torus and the star denoting the strong resonance in the I_1 direction coincide.

Bifurcation values for the parameters are now easily identified. First, we see that at $\alpha_2 = 0$, $h^+_{\min} = h^0_{\min} = h^p_{\min} = h_{par-res1} = 0$; namely, all the bifurcations mentioned above occur at one energy surface, and a double resonant (torus of fixed points in the 3 DOF case) normally parabolic torus is created, as shown in Figure 17B, where the star ($\omega_1 = 0$), the dotted line ($\omega_2 = 0$), and the circle (a parabolic torus) coincide. Then, the energy surface $H_0 = \alpha_2 = 0$ of system (7.1) shrinks to one 2-resonant normally parabolic 2-torus of fixed points. The existence of a double resonant parabolic torus is a codimension one phenomena for 3 DOF systems and a persistent phenomena in 4 or larger DOF systems [38]. Normally parabolic tori of fixed points are a codimension one phenomenon for any $n \geq 2$ (see [45, 38, 37] for more details).

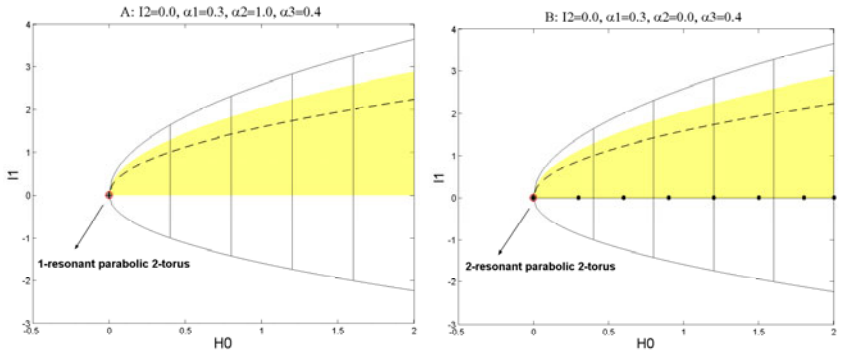

Figure 17. *2D slices of the EMBD at $I_2 = 0$. A: Regular parameter values—at $I_1 = H_0 = 0$ a resonance in the I_1 direction occurs. B: At the special bifurcation value $\alpha_2 = 0$. Since $\alpha_2 = 0$, at $I_1 = H_0 = 0$ a double resonance in the I_1 and I_2 direction occurs.*

Second, notice that

$$\frac{d^2 H_{bif}(\pm\sqrt{I_1}, 0, I_1, I_2)}{dI_1^2} = \mu_1; \tag{7.13}$$

hence, the fold of the singular surface $p^+_{ell}(h, I_1, I_2)$ in the I_1-direction becomes flatter as $\mu_1 \to 0$ (put differently, the dependence of the frequency $\omega_1^{\pm}$ on I_1 becomes weaker). It is seen that holding α_3 fixed in this limit changes the character of the energy surfaces from being bounded to being unbounded in I_1, I_2. We will not delve into the analysis of all the different limits which may be taken here; some of these limits are studied in detail in previous works (see [45, 46, 35, 36, 37, 38]). In particular, note that the appearance of flat parabolic resonant tori in such a situation gives rise to strong instabilities (see [38] and [37]).

7.2. The frequency domain plots (B). We plot the energy surfaces (ω^H) of the bifurcating system in the frequency space for typical and bifurcating energy values ($h^+_{\min}, h^0_{\min}, h^p_{\min}$, and $h_{par-res1}$ and h values in between them) with the resonance web plotted on them. We demonstrate that the structure of these webs differs from the structure of webs of a priori stable systems in its nonuniformity and its behavior near the origin.

The simplest type of energy surface component contains only elliptic lower dimensional tori. For $H_0 = h$, $h^+_{\min} < h < h^0_{\min}$, it appears as a smooth codimension one surface with boundaries, as shown in Figure 18, similar to Figure 6. This smooth compact component is a smooth deformation of the disk appearing in the energy-momentum space, (H_0, I_2, I_1). Transverse intersection of a smooth component of ω^H with one of the planes $\omega_j = 0$ corresponds to a strong resonance; for energy surfaces in the range $h^+_{\min} < h < h^0_{\min}$ this occurs only for $j = 1, 2$ (it cannot occur for $j = 0$ since in this energy range $\omega_0 > 0$). In Figure 18 (and in the following figures here) the red starred curve corresponds to the intersection of the energy surface, ω^H, with the resonance plane, $\omega_1 = 0$, and the black thick dotted line denotes the intersection of ω^H with $\omega_2 = 0$. The lower dimensional elliptic resonant tori correspond to the intersections of the surfaces' boundary, which is plotted in thick black, with the $\omega_j = 0$ ($j = 1$ or 2) planes.

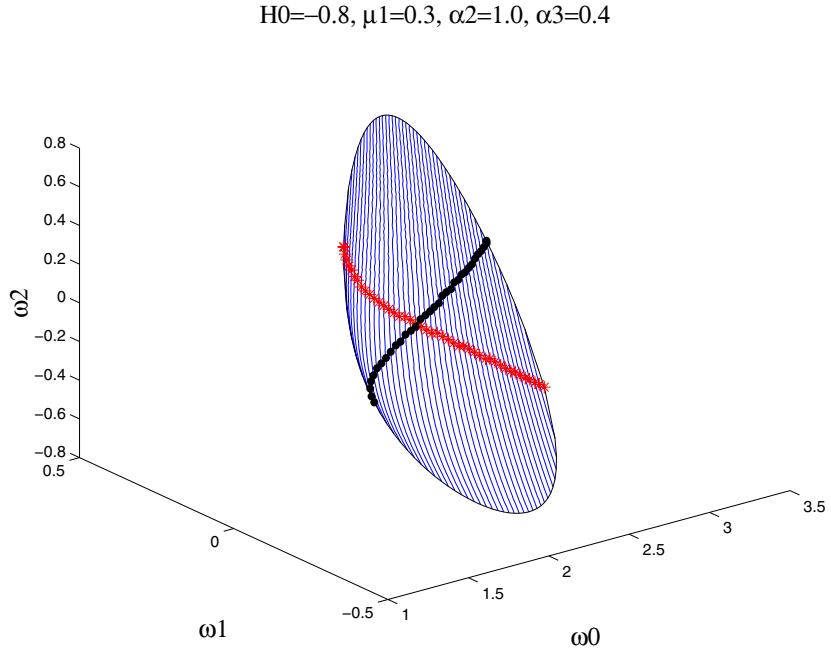

Figure 18. *A typical energy surface corresponding to an elliptic energy value $H_0 = h$ with $h^+_{\min} < h < h^0_{\min}$.*

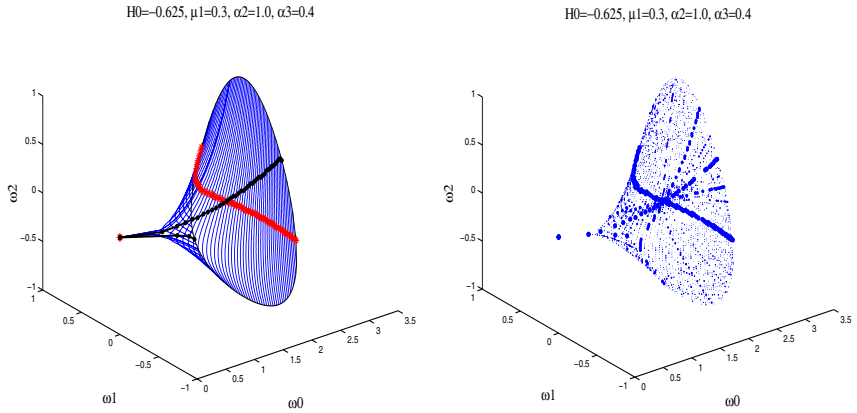

Figure 19. *An energy surface corresponding to the bifurcation value $H_0 = h^0_{\min}$, containing a double resonant hyperbolic torus of fixed points. Left: The frequency map plot. Right: The resonance web on this energy surface for $|k| \le 21$, where the size of the dots indicates the strength of the resonance.*

The energy value $H_0 = h^0_{\min}$ is a bifurcation value at which one 2-resonant hyperbolic 2-torus (hyperbolic torus of fixed points) appears. It creates a singular cusp point in the energy surface ω^H (see Figure 19), where this energy surface is presented in the three frequency space in the left plot (each blue thin curve corresponds to a fixed value of I_2, the red starred curve to the strong resonance $\omega_1 = 0$, the black dotted line to the strong resonance $\omega_2 = 0$, and the black thin curve to the boundary of ω_H, consisting of 2-tori) and the resonance web on

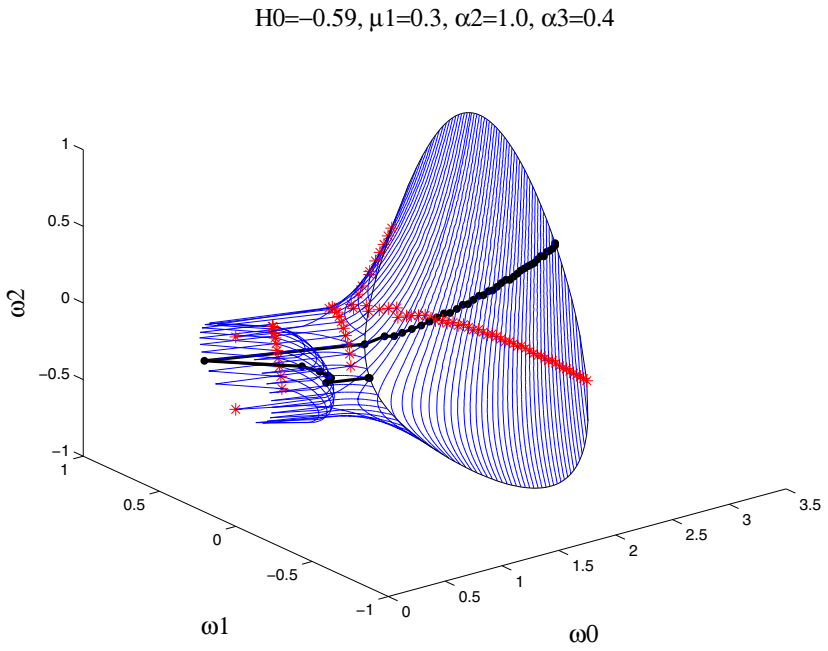

Figure 20. *A typical energy surface in the hyperbolic energy range, corresponding to an energy value $H_0 = h$ with $h^0_{\min} < h < h^p_{\min}$.*

this energy surface is presented in the right plot. The resonance webs presented here are calculated by finding (approximately) the points on the energy surface for which $\langle k, \omega^H \rangle = 0$ for $0 < |k| = |k_1| + |k_2| + |k_3| \leq 21$, where the size of the dots is in inverse relation to $|k|$; i.e., the stronger the resonance the larger the dot indicating it (note that for the weaker resonances the difference in the size of the dots is indistinguishable). The hyperbolic 2-resonant 2-torus in Figure 19 resides in the cusp, far from the other resonance lines and from the main resonance junction, where the strong resonances intersect (this might suggest an additional reason for not observing strong instabilities of the perturbed system near such hyperbolic double resonances [38]).

Energy surfaces with $H_0 = h$, $h^0_{\min} < h < h^p_{\min}$, include an ellipse of hyperbolic tori with their separatrices. As for the a priori unstable case, we find that the energy surface ω^H collides at this singular ellipse with the plane $\omega_0 = 0$ and then bounces back with the same sign of ω_0 (since the direction of motion does not change from the exterior to the interior tori). Using (7.12) and (7.10) we find that the singularity manifold corresponding to the family of hyperbolic 2-tori is given by

$$\begin{aligned} H_{bif}(0,0,I_1,I_2) &= H_{bif}(0,0,\omega_1,\omega_2) \\ &= \frac{1}{2}\frac{\left(\omega_1^0 - \alpha_3\omega_2\right)^2}{\mu_1 + \frac{1}{2} - \alpha_3^2} + \frac{1}{2}(\omega_2)^2 - \frac{1}{2}\alpha_2^2 - \frac{1}{2}\frac{(\alpha_2\alpha_3)^2}{\mu_1 + \frac{1}{2} - \alpha_3^2}. \end{aligned} \tag{7.14}$$

For our parameter range it is a tilted ellipse lying in the $\omega_0 = 0$ plane which is centered at the origin; see Figure 20 (similar to Figure 7).

On one side of this singularity manifold each point on the energy surface corresponds to two 3-tori, and on the other side to a single 3-torus as summarized by Figure 9C. Each of the surfaces $\omega_j = 0$ $(j = 1, 2)$ intersects the ellipse at two points, at hyperbolic 1-resonant 2-tori. In [38] we prove that such intersections are persistent. Recall that even though the singular circle is contained in the $\omega_0 = 0$ plane it does not correspond to a double resonance of the lower dimensional torus: $\omega_0 = 0$ at the homoclinic loop, whereas the normal frequency of the hyperbolic torus is imaginary and is nonzero.

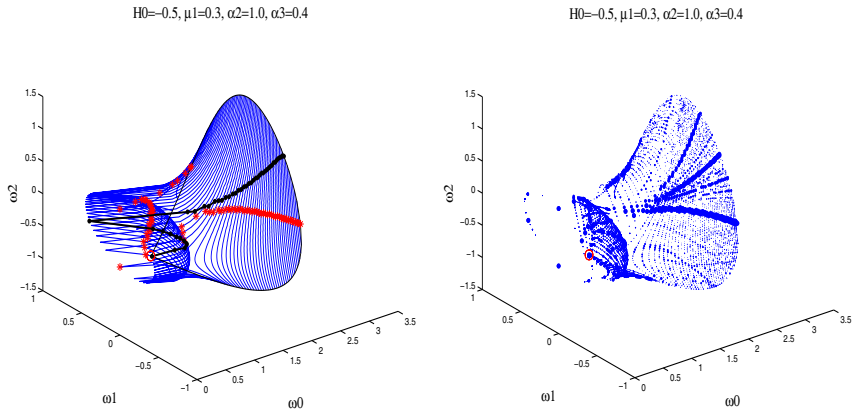

Figure 21. *An energy surface with $H_0 = h^p_{\min}$. Left: The energy surface in the frequency space. Right: The resonance web on this energy surface. Red circle: (Double) resonant (in the I_0- and I_2-directions) parabolic 2-torus.*

At the bifurcation value $H_0 = h^p_{\min}$ a parabolic (resonant in the I_2-direction) torus first appears; see Figure 21. An important observation is that *parabolic tori are a priori resonant*: their normal frequency vanishes. Indeed, let $\omega = (\Omega, \omega^{n-1}) \in \mathbb{R}^n$ denote the n dimensional vector of frequencies, including the normal frequency Ω, and the inner frequencies $(\omega^{n-1} \in \mathbb{R}^{n-1})$ of the $(n-1)$-torus. Parabolicity implies $\Omega = 0$; hence, $k^1 = e^1_n = (1, 0, \ldots, 0)$ satisfies the resonance condition $\langle k^1, \omega \rangle = 0$ (indeed, in the resonance web plots a large dot indicating strongest resonance always appears on the parabolic tori; see, e.g., Figure 21). Lower dimensional resonance implies that there exists at least one additional vector of integers, $k^2 = (0, l_{n-1}), l_{n-1} \in \mathbb{Z}^{n-1}$, such that $\langle k^2, \omega \rangle = 0$. Hence, *parabolic lower dimensional resonant tori correspond to junctions in the resonance web with at least one strongest resonance* (indeed, the parabolic torus in Figure 21 is doubly resonant, residing on the junction $\omega_0 = \omega_2 = 0$). In particular, if the parabolic torus appears at the origin, where all resonances intersect, it corresponds to an $(n-1)$-resonant $(n-1)$-torus, namely to a parabolic torus of fixed points. In [38] we prove that such a scenario is persistent in a one parameter family of integrable n DOF Hamiltonian systems with $n \geq 2$.

A typical energy surface in the energy range $H_0 = h$, $h^p_{\min} < h < h_{par-res1} = 0$, is shown in Figure 22 and in the range $H_0 = h > h_{par-res1} = 0$ in Figure 23, where the two parabolic tori are denoted by red circles. Then, the natural frequency in the xy-direction found from

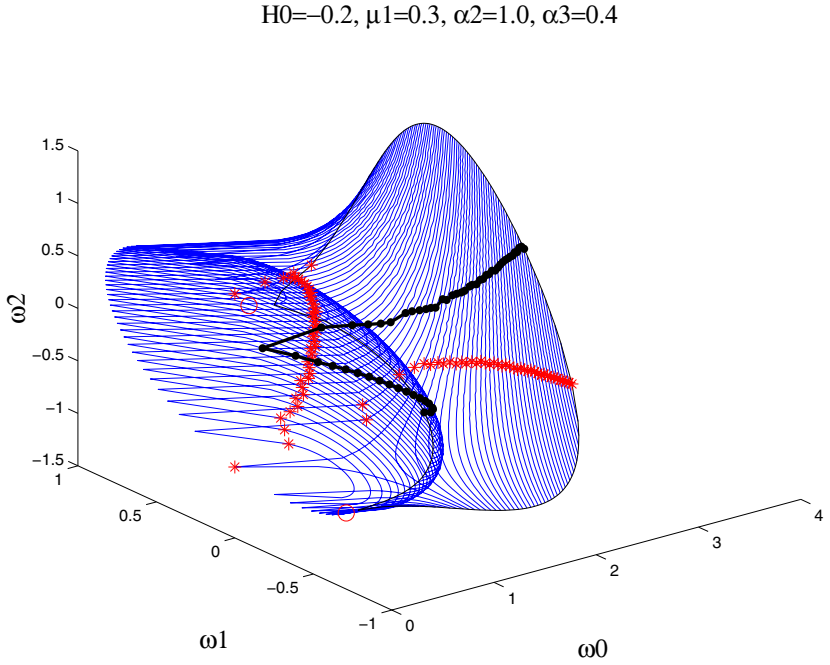

Figure 22. *A typical energy surface with* $h^p_{\min} < H_0 < 0$.

linearization at the origin,

$$\omega_0^0 = \sqrt{-I_1} = \sqrt{\frac{\omega_1^0 - \alpha_3\omega_2}{\mu_1 + \frac{1}{2} - \alpha_3^2} - \alpha_2\alpha_3},$$

shows that the singularity ellipse (7.14) detaches from the $\omega_0 = 0$ plane with a square-root distance. Topologically, the energy surface is well described by the branched surface in Figure 9E.

The colliding surface, at which ω^H is singular (nonsmooth), is clearly of codimension two, and it corresponds to the family of hyperbolic tori which live on the given energy surface. The end points of this collision surface, where the projection singularity heals and the energy surfaces cease to contain hyperbolic tori, correspond to parabolic tori, a codimension three surface, namely, points in Figures 9, 21, 22, 23, and 24 (the parabolic tori are denoted by red circles). At the parabolic lower dimensional tori the ω_0 frequency vanishes. If such an end surface (in the figures, a point) intersects another resonance surface, a parabolic (doubly) resonant torus is born. It is now clear that with additional DOF such an intersection (of the boundary of the collision surface and the resonances on the $\omega_0 = 0$ plane) is generically transverse (see [38] for a proof); hence parabolic resonances (PR) are expected to occur on surfaces corresponding to a range of energies. For the 3 DOF case, since generically the end points (corresponding to the inner frequencies of the parabolic tori) change continuously with the energy values, there exists a set of dense values of energies for which these end points hit resonance surfaces and PR are created. When an end point of a singularity curve belongs to

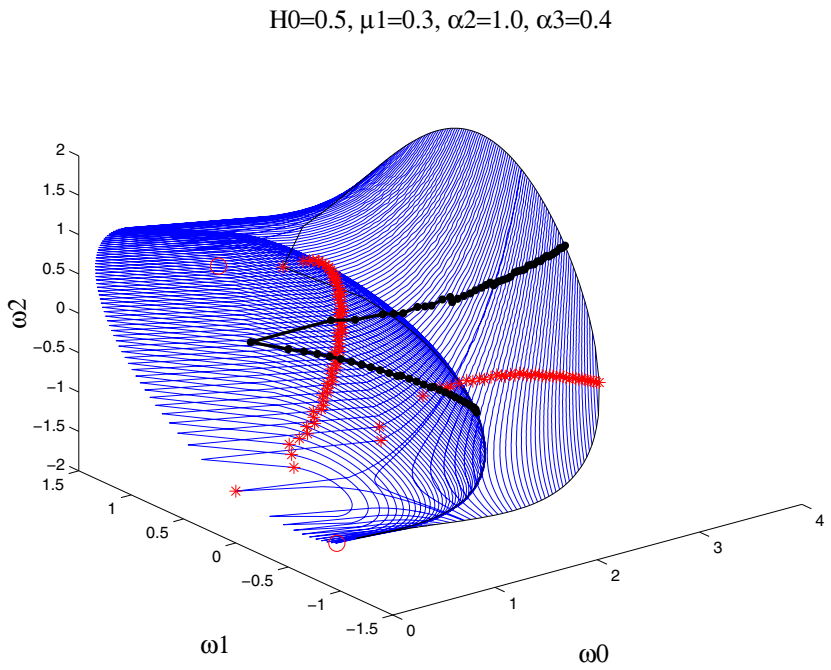

Figure 23. *A typical energy surface in the range* $H_0 > h^0_{par-res1} = 0$.

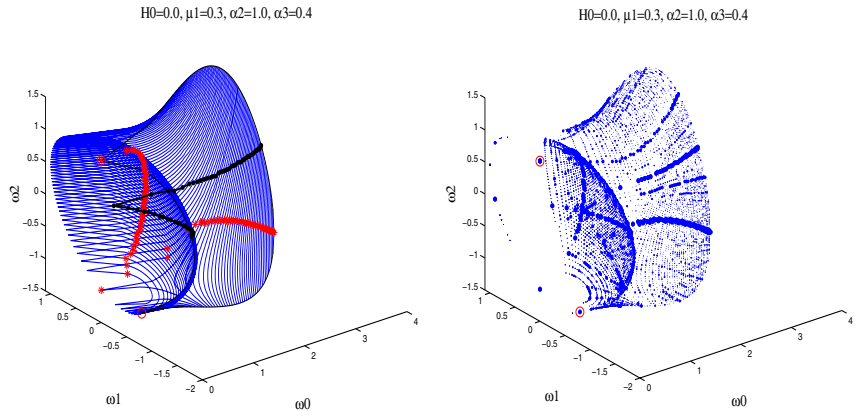

Figure 24. *An energy surface with* $H_0 = h_{par-res1} = 0$*, containing a strongly resonant in the* I_1 *direction parabolic* 2*-torus (hence, a double resonant parabolic torus). Left: This energy surface in the frequency space. Right: The resonance web on this energy surface.*

a strong resonance plane $\omega_j = 0$ ($j = 1$ or 2) it corresponds to a strong *double resonance* of the parabolic lower dimensional torus (see the resonance webs in Figures 21 and 24).

Figure 23 shows an energy surface for positive H_0, where the family of tori encircling the two wells crosses the $\omega_1 = 0$ plane. Figure 24 shows an energy surface with $H_0 = h_{par-res1} = 0$, which contains a resonant in the I_1 direction parabolic torus (hence strongly doubly resonant with $\omega_0 = \omega_1 = 0$) and the resonance web on this energy surface. Setting (in addition) $\alpha_2 = 0$,

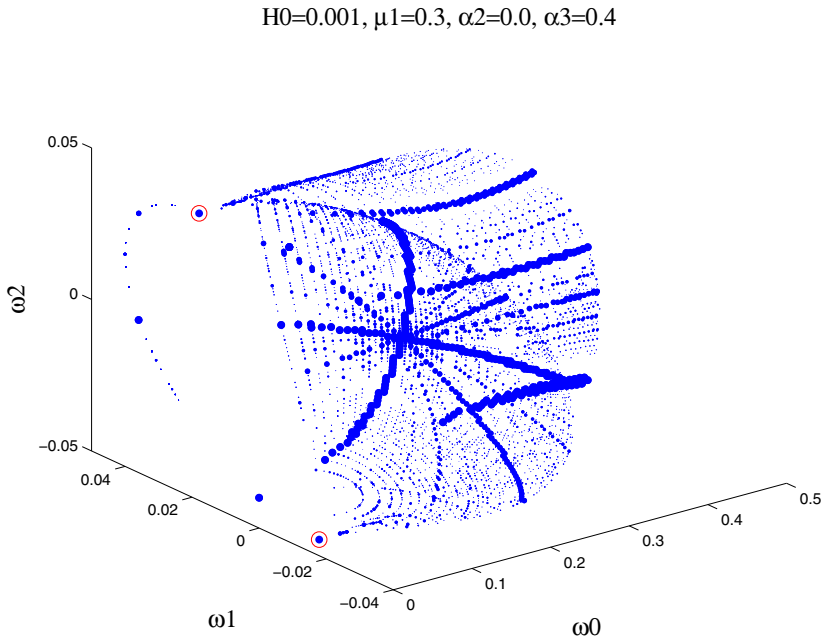

Figure 25. *A resonance web on an energy surface near the (locally KAM degenerate) energy surface with* $H_0 = \alpha_2 = 0$.

the energy surface with $H_0 = 0$ shrinks to a parabolic torus of fixed points at the origin of the frequency space. However, nearby energy surfaces (i.e., energy surfaces with $\alpha_2 = 0$ and a small energy value) have a nondiminishing extent in the frequency space, with resonant parabolic 2-tori residing near the main junction where many strong resonances intersect; see Figure 25 (note the scale of the axis).

Summarizing, we discovered that the presentation in the frequency space of the energy surfaces of Hamiltonians of the form $H_0(x, y, I)$ with $n-1$ dimensional tori that change their stability has the following properties:

- For a range of energies, the energy surface is singular along a codimension two surface belonging to the $\omega_0 = 0$ plane. This singularity surface corresponds to hyperbolic lower dimensional tori and their separatrices. The boundaries of the singularity surface (of codimension three) correspond to parabolic tori.
- Parabolic resonant tori may be recognized as resonance junctions which belong to the boundary of the hyperbolic singular surface. For 3 DOF systems these appear on a dense set of energy values; for $n \geq 4$ these appear for a range of energies.
- While the resonance surfaces still intersect the energy surfaces densely, the *uniformity seems to be lost*.
- A parabolic torus of fixed points appears when the boundary of the singular surface contains the origin. Such a scenario appears for special parameter values (a codimension one phenomena) and on specific energy surfaces.

7.3. Qualitative behavior of the near-integrable system (B). Using the plots of the EMBD we may read off all possible sources of instabilities. Here we need to combine several effects:

- Instabilities associated with the regular resonance web, as in the elliptic case.
- Instabilities associated with the existence of equi-energy family of separatrices and their resonances, as in the unstable case.
- Instabilities associated with resonant parabolic tori; their appearance implies the coexistence of equi-energy families of separatrices and equi-energy families of lower dimensional elliptic tori, meeting at the parabolic tori. The flatness of the singularity manifolds (see (7.13)) affects the extent of the instability.
- Instabilities associated with bifurcations in the structure of the singularity manifolds (manifolds corresponding to lower dimensional tori) of the energy surfaces—namely, the creation of elliptic, hyperbolic, and parabolic lower dimensional tori, all of which are associated with resonant lower dimensional tori.

Once again, the analysis of each of the above items has not been done yet. For the parabolic case we have mainly numerical indications for the behavior of the perturbed orbits; initial steps of a rigorous analysis of instabilities associated with PR are presented in [39] (a longer detailed version is in preparation). The behavior near a nonresonant parabolic torus does not yield instability—the lower dimensional parabolic torus persists [24]—and it appears that the behavior near it is indistinguishable from that appearing near the lower dimensional normally elliptic torus. However, numerical simulations indicate that the behavior near PR is dramatically different; orbits which appear to be chaotic and of a different nature than the homoclinic chaos are abundant. The structure of these perturbed orbits near 1-PR, which appear for a dense set of energy values, is similar to the one observed in the 2 DOF case; see [37, 45]. Further degeneracies make the instabilities more pronounced, see [37, 38] for examples.

One degeneracy we explore here is the existence of a normally parabolic torus of fixed points which is of codimension one ($\alpha_2 = 0$) and corresponds to *a local* violation of the KAM nondegeneracy condition. The induced strong instabilities of a perturbed orbit with initial values near this point are presented in Figures 26 and 27; in Figure 26 the perturbed orbit is projected on the (θ, I) planes, where its complicated structure, while it passes through the successive resonance zones, may be seen; in Figure 27 we show the development of the instabilities in the action variables depending on time. These figures were produced for the perturbed Hamiltonian:

$$H^{\varepsilon}_{bif}(x,y,\theta_1,I_1,\theta_2,I_2;\varepsilon) = \frac{y^2}{2} - \frac{x^2}{2}I_1 + \frac{x^4}{4} + \left(\mu_1 + \frac{1}{2}\right)\frac{I_1^2}{2} + \frac{I_2^2}{2} + \alpha_3 I_1 I_2 + \varepsilon\left(\left(1 - \frac{x^2}{2}\right)\cos(3\theta_1) + \cos(3\theta_2)\right). \tag{7.15}$$

Graphically, in the frequency space, such a scenario happens when the boundary of the singularity surface (here the end points of the singularity lines) passes through the origin, where all the resonance planes intersect. The fact that a parabolic 2-resonant torus resides at this junction point seems to induce strong instabilities in the perturbed system in both

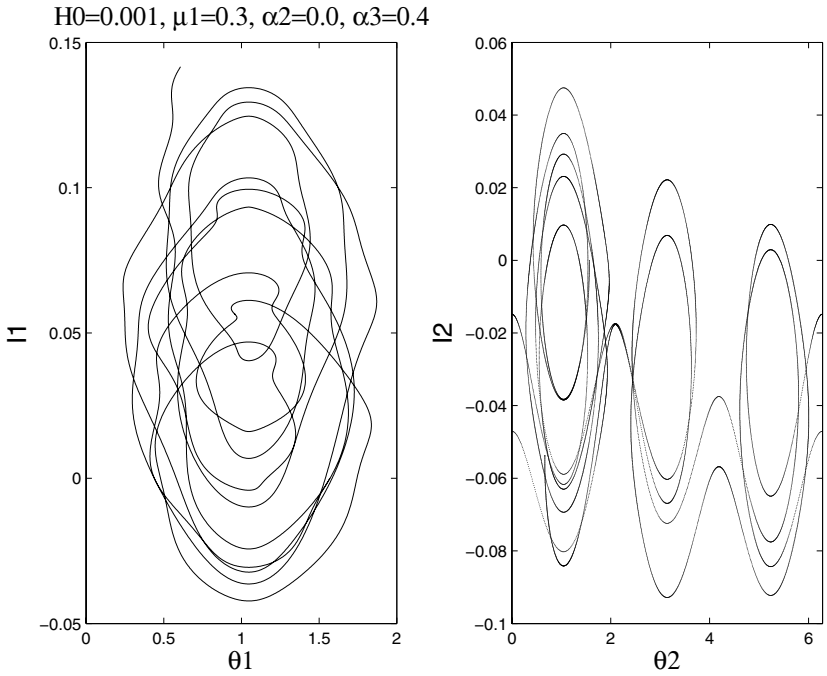

Figure 26. *Instability in the action variables near 2-PR: A perturbed orbit projected on the* (θ, I) *planes, corresponding to the total energy* $H \approx 9.953e-4$*, with initial conditions* $(x, y, \theta_1, I_1, \theta_2, I_2; \varepsilon) = (0.2515, 0, 1.57, 0, 1.57, 0, 1e-3, 1e-3)$.

action directions, as seen in Figures 26 and 27. In Figure 28 the corresponding unperturbed energy surface is shown in the (I_2, I_1) plane and in the frequency space (see the corresponding resonance web in Figure 25). The perturbed orbit shown in Figures 26 and 27 approximately covers the whole possible extent of the actions range on this surface. For more details and upper bounds on the maximal instability rate see [37, 38, 39]; in particular, in [39] analytical methods for studying instabilities near 2-PR are suggested.

Note that in 4 or more DOF systems the existence of a double resonant parabolic torus is persistent without dependence of the system on external parameters, and the local violation of the KAM iso-energetic nondegeneracy condition is avoided. Numerical simulations suggest that near such double PR the instabilities and the orbit structure are similar to the ones appearing in the locally degenerate 3 DOF system (with $\alpha_2 = 0$).

8. Bifurcations in the energy-momentum diagrams. Here we formulate the observed relations between bifurcations in the EMBD and the appearance of lower dimensional resonances precisely. First we prove that extrema of the nonparabolic singularity surfaces in the EMBD occur iff the corresponding tori are resonant. Then we prove that if on a given energy surface there exists an $(n-1)$-nonparabolic torus which is nondegenerately strongly $(n-1)$-resonant (see definitions below), then the topology of the energy surfaces changes at this value of the energy. We end with formulating similar results for the parabolic case. After stating the results for the generic parabolic case we show that our model Hamiltonian H_{bif}

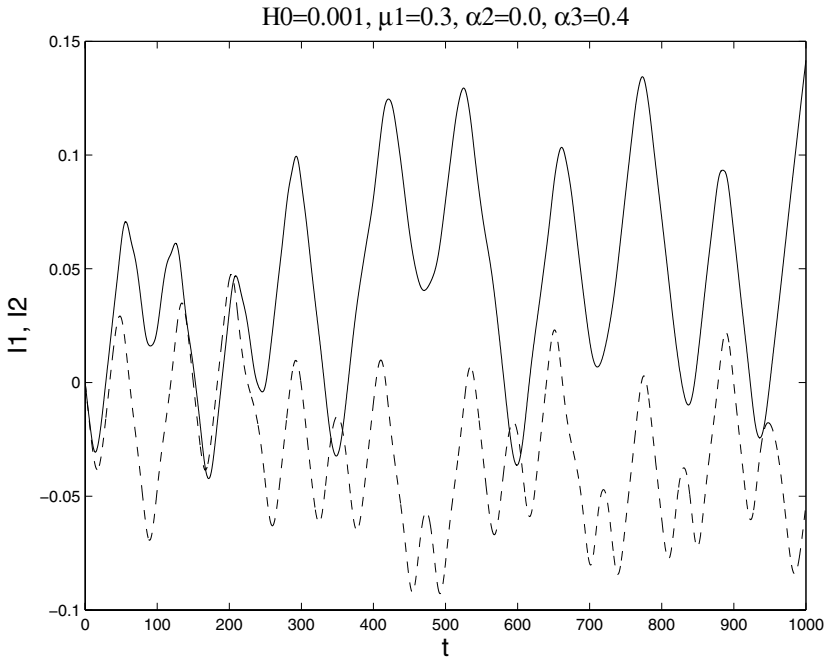

Figure 27. *Instability in the action variables near 2-PR: A perturbed orbit projected on the time-actions plane, with initial conditions as in Figure 26. Solid line: I_1. Dashed line: I_2.*

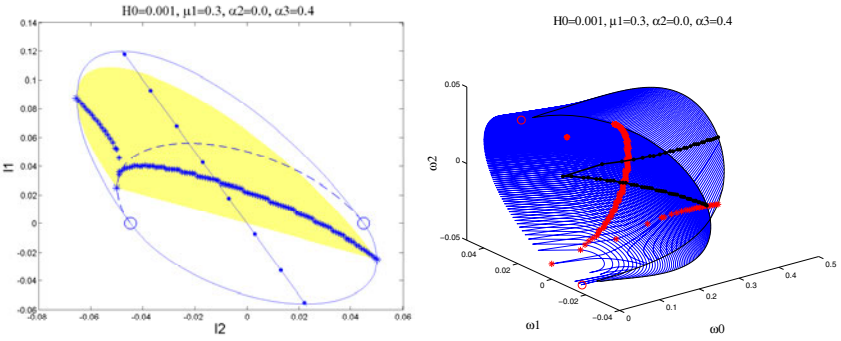

Figure 28. *An energy surface of H_{bif} with $\alpha_2 = 0$, $H_0 = 1e-3$. Left: An EMBD in the (I_2, I_1) plane. Right: In the frequency space.*

is nongeneric in this context (because of its Z_2 symmetry) and formulate the corresponding results to a suitable class of Hamiltonians.

8.1. Folds in the EMBD and resonances. Consider the EMBD near a singular family of $n-1$ lower dimensional tori, p_f. (Here we again take $s = 1$. General value of s will be considered elsewhere.) The unperturbed Hamiltonian, expressed in suitable local coordinates near p_f, is given by $H_0 = H_0(x, y, I)$, where $p_f = (x_f, y_f, I_f)$ satisfies $\nabla_{x,y} H_0(x, y, I)|_{p_f} = 0$. By the implicit function theorem (IFT), if the Hessian of H_0 with respect to x, y is nonsingular

at p_f (namely, $\det \frac{\partial^2 H(x,y,I)}{\partial x \partial y}|_{p_f} \neq 0$), we may express this manifold as a graph over the I variables: $p_f = (x_f(I), y_f(I), I)$. Then, apart from parabolic points (where $\det \frac{\partial^2 H(x,y,I)}{\partial x \partial y}|_{p_f} = 0$), p_f is represented in the EMBD by the codimension one smooth manifold $p_f^h = \{h_f(I), I\} = \{H_0(x_f(I), y_f(I), I), I\}$.[15] It is now natural to define extremal points of the singularity surface in the EMBD.

Definition 5. *p_f^c is a simple k-extremal point of the singularity manifold p_f^h if p_f^c is nonparabolic and $h_f(I) = H_0(x_f(I), y_f(I), I)$ has a local extremal in k directions at p_f^c; i.e., there exist $i_1, \ldots, i_k \in \{1, \ldots, n-1\}$ such that*

$$\left.\frac{\partial h_f(I)}{\partial I_i}\right|_{p_f^c} = 0 \text{ for } i = i_1, \ldots, i_k. \tag{8.1}$$

Theorem 1. *Consider a family of singular nonparabolic $n-1$ dimensional tori $p_f(I) = (x_f(I), y_f(I), I)$, where (x, y, I) are suitable coordinates near $p_f(I)$. Then $p_f^c = p_f(I^c)$ is a simple k-extremal point of the corresponding singularity manifold in the EMBD iff p_f^c corresponds to a k-strongly resonant lower dimensional torus.*

Proof. Since p_f^c is not parabolic the representation $p_f^h = \{h_f(I) = H_0(x_f(I), y_f(I), I), I\}$ is nonsingular near p_f^c. Hence, p_f^c is a k-extremal point iff the surface $\{h_f(I) = H_0(x_f(I), y_f(I), I), I\}$ in the (h, I) space is extremal in k directions $I_{i_1}, \ldots, I_{i_k}$ at p_f^c. This occurs, by definition, iff $\frac{\partial h_f(I)}{\partial I_i}$ vanishes in the corresponding k directions at p_f^c as expressed in (8.1). Since we use suitable coordinates, and since $\nabla_{x,y} H_0(x, y, I)|_{p_f} = 0$, it follows that for $i = i_1, \ldots, i_k$

$$\left.\dot{\theta}_i\right|_{p_f^c} = \left.\frac{\partial H(x,y,I)}{\partial I_i}\right|_{p_f^c} = \left.\frac{dH(p_f(I))}{dI_i}\right|_{p_f^c} = \left.\frac{\partial h_f(I)}{\partial I_i}\right|_{p_f^c} = 0. \tag{8.2}$$

■

Theorem 1 relates the extremal point of the singularity surfaces in the EMBD and resonances. We have seen that the topology of the energy surfaces changes at folds of these singular surfaces. We note here the triviality that folds imply extremum points, and extremum points with first nonvanishing derivatives of even order imply folds.

8.2. Topological bifurcations. In the previous section we saw that H_{bif} has two values $h_c = h_{ell}^+, h_{hyp}^0$ which are simple 2-fold points of the elliptic and hyperbolic singularity surfaces (namely, these singularity surfaces have an even order extrema in two action directions), several families of curves on which a simple 1-fold occurs (corresponding to the intersection of the singularity surfaces $p_{ell}^{\pm}, p_{hyp}^0, p_{ell}^0$ with the corresponding resonances), and $h_c = h_p^0$ is a 1-parabolic fold point corresponding to the first appearance of parabolic tori. We observe that h_{ell}^+, h_{hyp}^0, and h_p^0 correspond to a topological change in the energy surfaces' structure, namely, the corresponding topology of the branched surfaces changes across these energy values, but that the families along which a simple 1-fold occurs do not correspond to such changes. We would like to formulate these observations. First, we need to define the branched surfaces in a precise way.

[15] With a slight abuse of notation we denoted it in previous sections by $p_f = (h_f(I), I)$ as well (see, for example, (7.2), (7.3), (7.4)).

Recall that h_c is a topological bifurcation point if the branched surfaces across h_c are not equivalent (definition 3). If the topology of A_h^S, the singularity manifold for a given energy surface, changes across h, then the branched surfaces across h are not equivalent. Using the Morse lemma we establish that for $s = 1$ the singularity manifold, A_h^S, changes its topology near folds of the singularity surfaces. Since folds of the singularity surfaces imply extrema and extrema imply resonances, the main result follows.

Definition 6. *p_f^c is an $n-k$ $(0 < k < n)$ strongly resonant $n-1$ dimensional singular torus with nondegenerate frequency vector if in the suitable Arnold–Liouville–Nekhoroshev coordinates*

$$\frac{dH_0(p_f^c)}{dI_j} = 0, \quad \det\left(\frac{d^2H_0(p_f^c)}{dI_i dI_j}\right) \neq 0, \qquad j = 1, \dots, k. \tag{8.3}$$

The relation between (8.3) and resonances, as stated in the definition, follows from Theorem 1.

Theorem 2. *If p_f^c is a nonparabolic $n-1$ strongly resonant $n-1$ dimensional singular torus with a nondegenerate frequency vector, then $h_c = H_0(p_f^c)$ is a topological bifurcation point.*

Proof. The theorem essentially follows from the Morse lemma (see [26] or [41]); we include some details to enhance the intuition. Using the suitable coordinates near p_f, we may write

$$H_0(p_f - p_f^c) = H_0(p_f^c) + (I^f - I^c)^T A (I^f - I^c) + O(3), \tag{8.4}$$

where A is the Hessian at p_f^c : $A = \frac{d^2H_0(p_f^c)}{dI_i dI_j}$ (recall that $\nabla_{x,y} H_0(p_f - p_f^c) \equiv 0$). Hence, by linear orthonormal transformation $Uz = I$, we may write (8.4) as

$$H_0(p_f - p_f^c) - H_0(p_f^c) + \sum_{i=1}^{n-1-r} a_{i+r} z_{i+r}^2 = \sum_{i=1}^{r} a_i z_i^2 + O(3),$$

where $a_i > 0$ for all i by the nondegeneracy assumption. In fact, r is the Morse index of $h_f(I) = H_0(x_f(I), y_f(I), I)$ at p_f^c (the dimension of the subspace for which the Hessian A is positive definite). The Morse lemma, which applies to $h_f(I)$ by (8.3), states that by smooth local change of coordinates we can eliminate all higher order terms and set all the a_i's to unity. It follows immediately that intersection of the singularity surface $\{H_0(p_f), I_f\}$ with the plane $H_0(p_f) = h$ near p_f^c changes its topology across $h_c = H_0(p_f^c)$; if $r = n-1$ (resp., $r = 0$). Namely, if A is positive (negative) definite, then for $h < h_c$ $(h > h_c)$ there is no branch of p_f near p_f^c satisfying $H_0(p_f) = h$, whereas on the other side there is an $n-2$ dimensional ellipse satisfying this equation. If $0 < r < n-1$, the hyperboloids $p_f(h, \cdot)$ change their orientation at $h = h_c$; namely, they do not depend smoothly on h at h_c. Since the branched surfaces change across the surfaces $p_f(h, \cdot)$, the claim is proved. ∎

8.3. Parabolic tori and topological bifurcations. Consider the surface of parabolic lower dimensional tori $p_{pf} = (x_{pf}, y_{pf}, I_{pf})$ so that

$$\nabla_{x,y} H_0(x, y, I)|_{p_{pf}} = \det \left.\frac{\partial^2 H(x, y, I)}{\partial x \partial y}\right|_{p_{pf}} = 0. \tag{8.5}$$

These three equations define (generically) a codimension two surface in the EMBD, the singularity surface, p^h_{pf}. Along p^h_{pf} two (or more, in symmetric/degenerate cases) singularity surfaces representing families of nonparabolic $(n-1)$-tori, $p^h_{f_i}(I)$, $i = 1, \dots, n$, meet. For example, in section 7, the four singularity surfaces $p^h_{f_{1,2}}(I) = p^{\pm}_{ell}$, $p^h_{f_{3,4}}(I) = p^0_{hyp,ell}$ meet at $p^h_{pf} = p^0_{par}$. The natural oscillations in the xy plane of the $n-1$ dimensional tori p_{pf} vanish, so these tori are strongly resonant in the ω_0-direction. We now address the natural question in view of Theorem 1: When do extremal points of this singularity surface (p^h_{pf}) in the EMBD correspond to additional strong resonances? Here, one should take careful limits when considering derivatives across the singular boundary of $p^h_{f_i}(I)$, namely, across p^h_{pf}. To formulate such conditions let us investigate more fully (8.5). Define the functions

$$f_1(x,y,I) = \frac{\partial H(x,y,I)}{\partial x},\ f_2(x,y,I) = \frac{\partial H(x,y,I)}{\partial y},\ f_3(x,y,I) = \det \frac{\partial^2 H(x,y,I)}{\partial x \partial y};$$

then (8.5) defines the surface $f_1(x,y,I) = f_2(x,y,I) = f_3(x,y,I) = 0$. Can this surface be represented as a graph over the $n-2$ actions $J^{n-2} = (I_1, \dots, I_{j_p-1}, I_{j_p+1}, \dots, I_{n-1})$ for some chosen index j_p? By the IFT, this may be done if $\frac{\partial(f_1,f_2,f_3)}{\partial(x,y,I_{j_p})}$ is nonsingular, and hence we have the following definition.

Definition 7. *p_{pf} is an $n-1$ dimensional parabolic torus which is nondegenerate in the I_{j_p} direction if p_{pf} satisfies (8.5) and*

$$\det \frac{\partial(\frac{\partial H(x,y,I)}{\partial x}, \frac{\partial H(x,y,I)}{\partial y}, \det \frac{\partial^2 H(x,y,I)}{\partial x \partial y})}{\partial(x,y,I_{j_p})}\bigg|_{p_{pf}} \neq 0. \tag{8.6}$$

If p^*_{pf} is an $n-1$ dimensional parabolic torus which is nondegenerate in the I_{j_p}-direction, then in its neighborhood there is an $n-2$ dimensional family of parabolic tori p_{pf} which may be expressed as a graph over the $n-2$ actions $J^{n-2} = (I_1, \dots, I_{j_p-1}, I_{j_p+1}, \dots, I_{n-1}) : p_{pf}(J^{n-2}) = (x_{pf}(J^{n-2}), y_{pf}(J^{n-2}), I_{j_p}(J^{n-2}), J^{n-2})$. It follows that the corresponding codimension two surface in the EMBD can be represented as a graph over the same actions as well:

$$\begin{aligned} p^h_{pf}(J^{n-2}) &= \{H_0(x_{pf}(J^{n-2}), y_{pf}(J^{n-2}), I_{j_p}(J^{n-2}), J^{n-2}), I_{j_p}(J^{n-2}), J^{n-2}\} \\ &= \{h_{pf}(J^{n-2}), I_{j_p}(J^{n-2}), J^{n-2}\}. \end{aligned}$$

Using (8.5), it follows that

$$\begin{aligned} \frac{\partial h_{pf}(J^{n-2})}{\partial I_j}\bigg|_{p_{pf}} &= \left(\frac{\partial H(x,y,I)}{\partial I_j} + \frac{\partial H(x,y,I)}{\partial I_{j_p}} \frac{\partial I_{j_p}(J^{n-2})}{\partial I_j}\right)\bigg|_{p_{pf}} \\ &= \left(\dot\theta_j + \dot\theta_{j_p} \frac{\partial I_{j_p}(J^{n-2})}{\partial I_j}\right)\bigg|_{p_{pf}} \quad \text{for } j \neq j_p, \end{aligned} \tag{8.7}$$

whereas

$$\dot\theta_{j_p}\bigg|_{p_{pf}} = \frac{\partial H(x,y,I)}{\partial I_{j_p}}\bigg|_{p_{pf}} = \frac{\partial h_{f_i}(I)}{\partial I_{j_p}}\bigg|_{p_{f_i} \to p_{pf}}, \tag{8.8}$$

and the independence of the last term on i follows from the smooth dependence of the Hamiltonian flow on I, even across the parabolic (in the xy-direction) point. The relation between extremal points of $h_{pf}(J^{n-2})$ (at which $\frac{\partial h_{pf}(I)}{\partial I_i}|_{p_{pf}} = 0$) and resonances is now clear.

Theorem 3. *Consider a family of normally parabolic $n-1$ dimensional tori $p_{pf} = (x_{pf}, y_{pf}, I_{pf})$ which is nondegenerate in the I_{j_p}-direction at p^c_{pf}. Then, for $j \neq j_p$, an extremal point in the I_j-direction of the corresponding singularity manifold in the EMBD at p^c_{pf} corresponds to a strong resonance in this direction iff p^c_{pf} is strongly resonant in the I_{j_p}-direction or if I_{j_p} is extremal in I_j at p^c_{pf}. p^c_{pf} is strongly resonant in the I_{j_p}-direction iff the nonparabolic singularity surfaces emanating from p_{pf} are extremal in the I_{j_p}-direction in the limit $p_{f_i} \to p^c_{pf}$.*

An attempt to apply the above theorem to system (7.1) immediately fails—this system does not satisfy the nondegeneracy condition (8.6). Considering all systems with natural mechanical potential in the xy plane having a parabolic invariant $(n-1)$-torus at the origin,

$$H^{gen}_{bif}(x, y, I) = \frac{y^2}{2} - \frac{x^2}{2} f(I) + V(x, I), \tag{8.9}$$
$$f(0) = 0, \quad \left.\frac{\partial V}{\partial x}\right|_{(0,0)} = 0, \quad \left.\frac{\partial^2 V}{\partial x^2}\right|_{(0,0)} = 0,$$

shows that the nondegeneracy condition (8.6) corresponds to

$$\left.\frac{\partial^3 V}{\partial x^3}\frac{\partial^2 V}{\partial x \partial I_{j_p}}\right|_{(0,0)} \neq 0;$$

namely, the system is asymmetric with respect to reflections in x, and the location of the bifurcating invariant tori depends on I_{j_p}. Hence, any natural mechanical system with Z_2 symmetry does not satisfy (8.6).

We observe that another possibility (which is realized in our case of system (7.1)) of satisfying (8.5) along a simple $n-2$ dimensional surface is to require that the unperturbed system separates to a sum of two Hamiltonians, the first depending on (x, y, I_{j_p}) and the second depending on the actions $(I_1, \ldots, I_{n-1})$. In this case equations (8.5) are independent of $J^{n-2} = (I_1, \ldots, I_{j_p-1}, I_{j_p+1}, \ldots, I_{n-1})$, and any solution of these equations is satisfied for all J^{n-2} values. This separability assumption is of course highly nongeneric from a mathematical point of view but is certainly of physical relevance (a similar approach appears in the theory of partial averaging).

Definition 8. *p_{pf} is an $n-1$ dimensional parabolic torus fully degenerate in the I_{j_p}-direction if p_{pf} does not satisfy (8.6) but does satisfy (8.5) and these equations are independent of I_j for all $j \neq j_p$.*

This condition is satisfied for any system of the form (8.9) if $f(I) = f(I_{j_p}), V(x, I) = V(x, I_{j_p}) + g(I)$. In this case p_{pf} can be locally presented as the surface $(x_{pf}, y_{pf}, I_{j_p,pf}, J^{n-2})$ with $x_{pf}, y_{pf}, I_{j_p,pf}$ independent of J^{n-2} so $\frac{\partial I_{j_p,pf}}{\partial I_j} = 0$ for $j \neq j_p$. Indeed, for (7.1), we saw that $j_p = 1$ and $p_{pf} = (x_{pf}, y_{pf}, I_{1,pf}, I_2) = (0, 0, 0, I_2)$. Hence, near a parabolic torus, which is fully degenerate in the I_{j_p} direction, we can present the $n-2$ dimensional family of parabolic tori as $p^h_{pf}(J^{n-2}) = \{H_0(x_{pf}, y_{pf}, I_{j_p}, J^{n-2}), I_{j_p}, J^{n-2}\} = \{h_{pf}(J^{n-2}), I_{j_p}, J^{n-2}\}$. The relation

between extrema of $h_{pf}(J^{n-2})$ and additional resonances follows immediately from (8.7) and (8.8), where we use $\frac{\partial I_{j_p}}{\partial I_j} = 0$ to conclude the following.

Theorem 4. *Consider a family of normally parabolic $n-1$ dimensional tori $p_{pf} = (x_{pf}, y_{pf}, I_{pf})$, which is fully degenerate in the I_{j_p}-direction at p^c_{pf}. Then, for $j \neq j_p$, the extremal point in the I_j-direction of the corresponding singularity manifold in the EMBD at p^c_{pf} corresponds to a strong resonance in this direction. p^c_{pf} is strongly resonant in the I_{j_p}-direction iff the nonparabolic singularity surfaces emanating from p_{pf} are extremal in the I_{j_p}-direction in the limit $p_{f_i} \to p^c_{pf}$.*

As in section 8.2, by the Morse lemma, $n-2$ nondegenerate folds in the direction of the $n-2$ actions J^{n-2} of the codimension two surface $p^h_{pf}(J^{n-2})$ correspond to topological bifurcations. From (8.7) and (8.8) we conclude that such folds are not always associated with resonances, and we should distinguish between three cases.[16] For the fully degenerate case folds and resonances are simply related.

Theorem 5. *Consider an $n-1$ dimensional parabolic torus, p^c_{pf}. Assume p^c_{pf} is completely degenerate in the I_{j_p}-direction and that p^c_{pf} is $n-2$ strongly resonant with nondegenerate frequency vector in the $I_1, \ldots, I_{j-1}, I_{j+1}, \ldots, I_{n-1}$-directions; then $h_{pc} = H_0(p^c_{pf})$ is a topological bifurcation point.*

In section 7, the energy $h_{pc} = h^0_p$ is a topological bifurcation point which is well described by this theorem; at h^0_p parabolic tori first appear, and we have seen that a resonance in the I_2-direction occurs there.

In the generic case, a fold of $p^h_{pf}(J^{n-2})$ in the I_j-direction is associated with resonance if $\dot{\theta}_{j_p} = 0$ or if $\frac{\partial I_{j_p}(J^{n-2})}{\partial I_j}|_{p^c_{pf}} = 0$. Hence, topological bifurcations occurring at an $n-2$ fold of $p^h_{pf}(J^{n-2})$ are associated with a resonance only if additional conditions are satisfied. To satisfy these additional conditions in a persistent way the system must have additional parameters or symmetries.

Theorem 6. *Consider an $n-1$ dimensional parabolic torus, p^c_{pf}. Assume that p^c_{pf} is nondegenerate in the I_{j_p}-direction and that the Hamiltonian at p^c_{pf} is locally separable, namely, $\frac{\partial I_{j_p}(J^{n-2})}{\partial I_j}|_{p^c_{pf}} = 0$ for all $j \neq j_p$. Then, if p^c_{pf} is $n-2$ strongly resonant with nondegenerate frequency vector in the $I_1, \ldots, I_{j-1}, I_{j+1}, \ldots, I_{n-1}$-directions, then $h_{pc} = H_0(p^c_{pf})$ is a topological bifurcation point. Without imposed symmetries, such a phenomenon is of codimension $n-2$.*

Theorem 7. *If p^c_{pf} is an $n-1$ dimensional parabolic torus of fixed points which is nondegenerate in the I_{j_p}-direction and has nondegenerate frequency vector in the $I_1, \ldots, I_{j-1}, I_{j+1}, \ldots, I_{n-1}$-directions then $h_{pc} = H_0(p^c_{pf})$ is a topological bifurcation point. Without imposed symmetries, such a phenomenon is of codimension one.*

9. Discussion. We have shown that when the generalized action-angle coordinates can be extended globally (as in our prototype models of normally stable, unstable, and bifurcating

[16] Note that there are two different (independent) types of nondegeneracies. One corresponds to the standard assumption regarding changes in the frequency vector (Definition 6) and is needed for applying the Morse lemma. The other corresponds to the nondegenerate (degenerate) dependence of the parabolic tori on a specific action (Definitions 7,8).

tori) the combination of the EMBD and the branched surfaces supply global qualitative description of the *near-integrable* dynamics; on these diagrams the topological changes in the energy surfaces and the appearance of lower dimensional resonances are apparent, and thus various mechanisms for instabilities (such as homoclinic orbits, hyperbolic resonances, and PR) may be clearly identified. In particular, we proved that topological bifurcations of the energy surfaces correspond to folds of singularity surfaces in these diagrams and hence to resonances. In other works [37, 38] we have demonstrated that the curvature of these singularity surfaces at the folds plays a crucial role in the extent of the instabilities in the perturbed system. Again, such effects are easily identified in these diagrams.

Many issues remain for future studies:

- We have seen (sections 6.3 and 7.3) that there is a long list of instabilities associated with the near-integrable motion near families of lower dimensional tori which is not well understood yet.
- For 2 DOF systems, the description of the energy surfaces as graphs gives a useful insight regarding the evolution of the instabilities in the action variables (or, more generally, in the adiabatic variables of the system) under small conservative perturbations or conservative noise [20]. These ideas were generalized to n DOF systems with strong conservative noise which destroys all integrals of motion and small nonconservative noise which leads to diffusion between different energy surfaces [19]. In view of our work, one is lead naturally to investigation of motion in integrable (or near-integrable) systems with small conservative noise by studying *random motion along branched surfaces*.
- The behavior of systems for which the local generalized action-angle coordinates cannot be globally extended is yet to be studied. In particular, one would like to extend the presentation here so it will be applicable to the work of Fomenko and coworkers in which the topology of complicated systems, like the rigid body, is fully analyzed [17, 18]. On one hand, one may use general constants of motion plots in a similar fashion to what we have proposed for the EMBD, yet the relation between folds and resonances will be lost. On the other hand, even for such plots, finding the branched surfaces topology from the Fomenko graphs is challenging.
- The restriction to systems with compact level sets excludes important examples such as the Kepler problem. Delicate issues related to the possible appearance of noncompact critical level sets and singularities of the potential need to be addressed (see [47]).
- Notice that the generalized action-angle local representation naturally leads to investigation of the Hamiltonian function evaluated along the singularities as a function of the $n - s$ actions. Hence, as noted in [33], singularity theory may be used to classify all persistent bifurcations in the s DOF subsystem. Here, we further observe that resonances are also associated with singularities of this function. Full classification, as had been achieved for some of the bifurcation scenarios, is yet to be developed.
- Finally, the effect of $n-s$ dimensional tori with various stabilities in the $2s$ dimensional normal space for $s > 1$ (as in [33]) on the EMBD structure and the branched surfaces structure is yet to be understood.

Acknowledgments. It is a pleasure to thank Amadeu Delshams, Heinz Hanßmann, Rafael de la Llave, and Terre Seara for fruitful discussions.

REFERENCES

[1] R. Abraham and J. E. Marsden, *Foundations of Mechanics*, 2nd ed., Benjamin/Cummings Publishing, Reading, MA, 1978.
[2] V. I. Arnol'd, *Dynamical Systems* III, 2nd ed., Encyclopaedia Math. Sci. 3, Springer-Verlag, Berlin, 1993.
[3] S. V. Bolotin and D. V. Treschev, *Remarks on the definition of hyperbolic tori of Hamiltonian systems*, Regul. Chaotic Dyn., 5 (2000), pp. 401–412.
[4] A. V. Bolsinov and A. T. Fomenko, *Trajectory classification of simple integrable Hamiltonian systems on three-dimensional surfaces of constant energy*, Dokl. Akad. Nauk, 332 (1993), pp. 553–555 (in Russian). English translation in Russian Acad. Sci. Dokl. Math., 48, (1994), pp. 365–369.
[5] H. W. Broer, G. B. Huitema, and M. B. Sevryuk, *Quasi-Periodic Tori in Families of Dynamical Systems: Order Amidst Chaos*, Lecture Notes in Math. 1645, Springer-Verlag, New York, 1996.
[6] R. Cushman, *The momentum mapping of the harmonic oscillator*, in Symposia Mathematica, Vol. 14, Academic Press, London, 1974, pp. 323–342.
[7] R. H. Cushman and L. M. Bates, *Global Aspects of Classical Integrable Systems*, Birkhäuser Verlag, Basel, 1997.
[8] A. Delshams, R. de la Llave, and T. M. Seara, *A geometric approach to the existence of orbits with unbounded energy in generic periodic perturbations by a potential of generic geodesic flows of* $\mathbb{T}^2$, Comm. Math. Phys., 209 (2000), pp. 353–392.
[9] A. Delshams, R. de la Llave, and T. M. Seara, *A geometric mechanism for diffusion in Hamiltonian systems overcoming the large gap problem: Announcement of results*, Electron. Res. Announc. Amer. Math. Soc., 9 (2003), pp. 125–134.
[10] H. R. Dullin, M. Juhnke, and P. H. Richter, *Action integrals and energy surfaces of the Kovalevskaya top*, Internat. J. Bifur. Chaos Appl. Sci. Engrg., 4 (1994), pp. 1535–1562.
[11] H. R. Dullin, P. H. Richter, and A. P. Veselov, *Action variables of the Kovalevskaya top*, Regul. Chaotic Dyn., 3 (1998), pp. 18–26.
[12] L. H. Eliasson, *Perturbations of stable invariant tori for Hamiltonian systems*, Ann. Scuola Norm. Sup. Pisa Cl. Sci. (4), 15 (1988), pp. 115–147.
[13] N. Fenichel, *Persistence and smoothness of invariant manifolds for flows*, Indiana Univ. Math. J., 21 (1971), pp. 193–225.
[14] N. Fenichel, *Asymptotic stability with rate conditions*, Indiana Univ. Math. J., 23 (1974), pp. 1109–1137.
[15] N. Fenichel, *Asymptotic stability with rate conditions,* II, Indiana Univ. Math. J., 26 (1977), pp. 81–93.
[16] A. T. Fomenko, *Topological classification of all integrable Hamiltonian differential equations of general type with two degrees of freedom*, in The Geometry of Hamiltonian Systems, Math. Sci. Res. Inst. Publ. 22, Springer-Verlag, New York, 1991, pp. 131–339.
[17] A. T. Fomenko, Ed., *Topological classification of integrable systems*, Advances in Soviet Mathematics 6, AMS, Providence, RI, 1991.
[18] A. T. Fomenko, Ed., *Symplectic topology of integrable dynamical systems. Rough topological classification of classical cases of integrability in the dynamics of a heavy rigid body*, Zap. Nauchn. Sem. S.-Peterburg. Otdel. Mat. Inst. Steklov. (POMI), 235 (1996), pp. 104–183, 305. Translation in J. Math. Sci. (New York), 94 (1999), pp. 1512–1557.
[19] M. Freidlin and M. Weber, *On random perturbations of Hamiltonian systems with many degrees of freedom*, Stochastic Process. Appl., 94 (2001), pp. 199–239.
[20] M. I. Freidlin and A. D. Wentzell, *Random perturbations of Hamiltonian systems*, Mem. Amer. Math. Soc., 109 (1994).
[21] S. M. Graff, *On the conservation of hyperbolic invariant tori for Hamiltonian systems*, J. Differential Equations, 15 (1974), pp. 1–69.
[22] J. Guckenheimer and P. Holmes, *Nonlinear Oscillations, Dynamical Systems, and Bifurcations of Vector Fields*, Springer-Verlag, New York, 1983.

[23] G. Haller, *Chaos Near Resonance*, Appl. Math. Sci. 138, Springer-Verlag, New York, 1999.
[24] H. Hanßmann, *The quasi-periodic center-saddle bifurcation*, J. Differential Equations, 142 (1997), pp. 305–370.
[25] H. Hanßmann, *A survey on bifurcations of invariant tori*, in New Advances in Celestial Mechanics and Hamiltonian Systems, J. Delgado et al., eds., Kluwer Academic Publishers, Dordrecht, The Netherlands, 2004, pp. 109–121.
[26] A. Katok and B. Hasselblatt, *Introduction to the Modern Theory of Dynamical Systems*, Encyclopedia Math. Appl. 54, Cambridge University Press, Cambridge, UK, 1995.
[27] J. Laskar, *Frequency analysis for multi-dimensional systems. global dynamics and diffusion*, Phys. D, 67 (1993), pp. 257–281.
[28] J. Laskar, *Global dynamics and diffusion*, Phys. D, 67 (1993), pp. 257–281.
[29] L. Lerman, *Isoenergetical structure of integrable Hamiltonian systems in an extended neighborhood of a simple singular point: Three degrees of freedom*, Amer. Math. Soc. Transl. Ser. 2, 200 (2000), pp. 219–242.
[30] L. Lerman and Y. L. Umanskii, *Classification of four dimensional integrable Hamiltonian systems and Poisson actions of $\mathbb{R}^2$ in extended neighborhood of simple singular points,* I, Sb. Math., 77 (1994), pp. 511–542.
[31] L. Lerman and Y. L. Umanskii, *Classification of four dimensional integrable Hamiltonian systems and Poisson actions of $\mathbb{R}^2$ in extended neighborhood of simple singular points,* II, Sb. Math., 78 (1994), pp. 479–506.
[32] L. M. Lerman and Y. L. Umanskii, *Classification of four-dimensional integrable Hamiltonian systems and Poisson actions of $\mathbb{R}^2$ in extended neighborhoods of simple singular points.* III. *Realizations*, Mat. Sb., 186 (1995), pp. 89–102 (in Russian). English translation in Sb. Math., 186 (1995), pp. 1477–1491.
[33] L. M. Lerman and Y. L. Umanskii, *Four-dimensional integrable Hamiltonian systems with simple singular points (topological aspects)*, Transl. Math. Monogr. 176, AMS, Providence, RI, 1998. Translated from the Russian manuscript by A. Kononenko and A. Semenovich.
[34] A. Lichtenberg and M. Lieberman, *Regular and Stochastic Motion*, Appl. Math. Sci. 38, Springer-Verlag, New York, 1983.
[35] A. Litvak-Hinenzon, *Parabolic Resonances in Hamiltonian Systems*, Ph.D. thesis, The Weizmann Institute of Science, Rehovot, Israel, 2001.
[36] A. Litvak-Hinenzon and V. Rom-Kedar, *Parabolic resonances in near integrable Hamiltonian systems*, in Stochaos: Stochastic and Chaotic Dynamics in the Lakes, D. S. Broomhead, E. A. Luchinskaya, P. V. E. McClintock, and T. Mullin, eds., American Institute of Physics, Melville, NY, 2000, pp. 358–368.
[37] A. Litvak-Hinenzon and V. Rom-Kedar, *Parabolic resonances in 3 degree of freedom near-integrable Hamiltonian systems*, Phys. D, 164 (2002), pp. 213–250.
[38] A. Litvak-Hinenzon and V. Rom-Kedar, *Resonant tori and instabilities in Hamiltonian systems*, Nonlinearity, 15 (2002), pp. 1149–1177.
[39] A. Litvak-Hinenzon, *The Mechanism of Parabolic Resonance*, in Equadiff 2003, Hasselt, Belgium, J. Mawhin and S. V. Lunel, eds., World Scientific, Singapore, to appear.
[40] K. R. Meyer and R. G. Hall, *Introduction to Hamiltonian Dynamical Systems and the N-Body Problem*, Appl. Math. Sci. 90, Springer-Verlag, New York, 1991.
[41] J. Milnor, *Morse Theory. Based on Lecture Notes by M. Spivak and R. Wells*, Ann. of Math. Stud. 51, Princeton University Press, Princeton, NJ, 1963.
[42] N. N. Nehorošev, *Action-angle variables, and their generalizations*, Trans. Moscow Math. Soc., 26 (1972), pp. 181–198.
[43] A. A. Oshemkov, *Description of isoenergetic surfaces of integrable Hamiltonian systems with two degrees of freedom*, Trudy Sem. Vektor. Tenzor. Anal., 23 (1988), pp. 122–132 (in Russian).
[44] J. Pöschel, *On elliptic lower dimensional tori in Hamiltonian systems*, Math. Z., 202 (1989), pp. 559–608.
[45] V. Rom-Kedar, *Parabolic resonances and instabilities*, Chaos, 7 (1997), pp. 148–158.
[46] V. Rom-Kedar, Y. Dvorkin, and N. Paldor, *Chaotic Hamiltonian dynamics of particle's horizontal motion in the atmosphere*, Phys. D, 106 (1997), pp. 389–431.
[47] S. Smale, *Topology and mechanics.* I, Invent. Math., 10 (1970), pp. 305–331.

[48] J. L. Tennyson, M. A. Lieberman, and A. J. Lichtenberg, *Diffusion in near-integrable Hamiltonian systems with three degrees of freedom*, in Nonlinear Dynamics and the Beam-Beam Interaction AIP Conf. Proc. 57, Amer. Inst. Phys., New York, 1980, pp. 272–301.
[49] D. Treschev, *Multidimensional symplectic separatrix maps*, J. Nonlinear Sci., 12 (2002), pp. 27–58.
[50] D. Treschev, *Trajectories in a neighbourhood of asymptotic surfaces of a priori unstable Hamiltonian systems*, Nonlinearity, 15 (2002), pp. 2033–2052.
[51] H. Waalkens and H. R. Dullin, *Quantum monodromy in prolate ellipsoidal billiards*, Ann. Physics, 295 (2002), pp. 81–112.